Composite Structures 345 (2024) 118374

Contents lists available at ScienceDirect

Composite Structures

journal homepage: www.elsevier.com/locate/compstruct

Efficient equilibrium-based stress recovery for isogeometric laminated Euler–Bernoulli curved beams

Alessia Patton [a,*], Shirko Faroughi [b], Alessandro Reali [c]

[a] Department of Civil Engineering and Environmental Sciences - Universität der Bundeswehr München, Werner-Heisenberg-Weg 39, Neubiberg, 85577, Germany
[b] Department of Mechanical Engineering - Urmia University of Technology, Urmia, Iran
[c] Department of Civil Engineering and Architecture - University of Pavia, via Ferrata 3, Pavia, 27100, Italy

ARTICLE INFO

Keywords:
Laminated composite structures
Curved Euler–Bernoulli beams
Stress-recovery
Equilibrium
Isogeometric analysis
Collocation methods

ABSTRACT

Laminated curved composite parts, used, e.g., in the spar and ribs in aircraft and wind turbine blades, are typically subjected to high interlaminar stresses. This work focuses on a two-step procedure to study laminated Euler–Bernoulli curved beams discretized *via* Isogeometric Analysis (IGA). First, we solve a (planar) Euler–Bernoulli curved beam formulation in primal form to obtain the tangential and transverse displacements. This formulation features high-order PDEs, which we can straightforwardly approximate using either an IGA-Galerkin or an IGA-collocation approach. Starting from the obtained displacement solution, which accounts for bending-stretching coupling, we can directly compute the normal stress only, while we do not have information concerning the transverse shear stress state, typically responsible for delamination. However, by imposing equilibrium in strong form in a curvilinear framework which eases the post-processing, eliminating the need for coordinate changes, we can easily recover interlaminar transverse shear stresses at locations of interest. Such *a posteriori* step requires calculating the high-order displacement derivatives in the equilibrium equations and, therefore, demands once again higher-order regularity that can be easily fulfilled by exploiting the high-continuity properties of IGA. Extensive numerical tests prove the effectiveness of the proposed approach, which is also aided by the IGA's superior geometric approximation.

1. Introduction

Composite materials typically exhibit higher strength- and stiffness-to-weight ratios than most traditional materials like metals and plastics [1,2]. In recent years, there has been a growing interest in their usage in the aerospace and automotive industries as they provide the flexibility to achieve specific design objectives by optimizing, e.g., different stacking sequences. Curved beam components, which can be found in applications such as rotor blades of marine vessels and helicopters, civil structures like bridges, and various aerospace elements [3], are among the structures that benefit from the advantages deriving from composite peculiarities. Laminated composite curved beams often display a complex stress response even when subjected to simple loading conditions, primarily due to a possible mismatch in terms of material properties belonging to different layers. This stress state occurring through the laminate thickness may eventually lead to a mode of failure termed "delamination", which refers to the separation of layers along ply interfaces [4,5]. To address and prevent delamination, it is crucial to accurately predict the stress fields in these structures [6,7], focusing on the correct evaluation of the two or three-dimensional stress state throughout the composites thickness [4,5]. In the literature, various theories have been proposed for the analysis of curved laminated beams. Reddy [8] developed a third-order shear deformation theory to study laminated composite plates. This theory was further refined by Khdeir and Reddy [9] for investigating cross-ply laminated beams/arches. Kim [10] introduced a composite laminated hybrid-mixed curved beam element based on the Hellinger–Reissner variational principle and incorporating the first-order shear deformation theory. In [11], a linear Euler–Bernoulli model was employed to analyze the static and dynamic behavior of non-homogeneous symmetrical-cross-section curved beams and closed rings. Kant et al. [12] proposed a semi-analytical methodology providing an accurate stress analysis of composite and sandwich narrow beams. In [13], a 3D elastic total Lagrangian formulation was developed to investigate steel-concrete curved beams. Nguyen [14] studied the variation of tangential and radial stresses using a 3D finite element model for both isotropic and orthotropic curved laminated beams. Luu et al. [15] studied the non-dimensional deflection and critical buckling loads of shear deformable laminated

* Corresponding author.
E-mail addresses: alessia.patton@unibw.de (A. Patton), sh.farughi@uut.ac.ir (S. Faroughi), alessandro.reali@unipv.it (A. Reali).

https://doi.org/10.1016/j.compstruct.2024.118374
Received 30 March 2024; Received in revised form 24 June 2024; Accepted 5 July 2024
Available online 10 July 2024

composite curved beams. Ye et al. [16] and Mohamad et al. [17] investigated the vibration analysis of laminated composite curved beams under various boundary conditions, whereas Guo et al. [18] introduced a domain decomposition approach to analyze the static and free vibration behavior of curved beams. Instead, Hajianmaleki and Qatu [19] utilized the Timoshenko beam theory to study free vibrations in generally laminated deep curved beams under different boundary conditions. Thurnherr et al. [7] developed a higher-order beam model to investigate the flexural response of curved beams with constant curvature and arbitrary constant thickness. This model is derived from the Hellinger–Reissner mixed variational principle and ensures inherently equilibrated 3D stresses through an equivalent single-layer model. Yasin et al. [20] developed a third-order efficient layerwise theory for laminated composite and sandwich curved beams with deep curvatures. The circumferential displacement is assumed to exhibit a global third-order variation through-the-thickness coordinate with a linear plywise distribution. Avhad et al. [21] investigated the static analysis of laminated composite and sandwich curved beams using a novel quasi-3D polynomial-type beam theory, which accounts for the effects of both transverse shear and normal strains, including thickness-stretching effects. Other approximation theories of laminated composite structures comprise the "Carrera Unified Formulation" (CUF) [22]. CUF models allow control over the theory order, a flexible parameter that can be chosen through convergence analysis [23]. Filippi et al. [24], e.g., applied CUF to analyze functionally graded material beams for the first time. Based on the reported literature review, it is clear that various researchers have conducted extensive research on the static and vibration analysis of curved beams using first- and higher-order shear deformation theories. Additionally, specific models in the literature especially address the investigation of interlaminar stresses for those types of structures generally in the finite element context. Kress et al. [25] developed a model to investigate radial stresses in moderately thick curved laminates. Roos et al. [26] further enhanced this model by considering interlaminar shear stresses. In [27], a semi-analytical approach is reported for evaluating interlaminar stresses in curved beams with constant curvature. Kant and Swaminathan [28] presented a review of techniques able to analyze transverse/interlaminar stresses in multilayered plates and shells, underlining that a 2D-3D global/local finite element method (FEM) can drastically improve the overall computational efficiency.

A higher-order numerical approach alternative to FEM is isogeometric analysis (IGA) [29], which has shown a better accuracy per degree-of-freedom, an enhanced robustness with respect to standard finite elements, and a significant adaptability to various discretization schemes. IGA utilizes the same basis functions, namely smooth functions typically belonging to Computer-Aided Design (such as B-Splines or Non-uniform rational B-Splines (NURBS)), to approximate both the geometry and field variables, thereby tightly connecting design and analysis. IGA leads to an overall cost-saving simplification of the typically separated mesh generation and refinement procedures required in standard FEM, resulting in significant time and cost savings, and has demonstrated its effectiveness in solving a wide range of solid and structural problems, including the successful modeling of composite and sandwich beams. Dvořáková and Patzák [30] introduced an isogeometric Euler–Bernoulli straight beam element that provides an exact representation of concentrated loads. Luu et al. [31] developed a NURBS-based IGA method to study the free vibration behavior of generally laminated Timoshenko-type beams with arbitrary curvature. Faroughi et al. [32] formulated a displacement-only NURBS-based beam element, whereas Shafei et al. [33] utilized a third-order shear deformation theory to study vibration analysis in laminated composite beams. Marchiori and Neto [34] proposed an IGA formulation for 2D curved beams based on Euler–Bernoulli assumptions. Osterle et al. [35] presented a class of IGA formulations for beams, plates, and shells, which intrinsically avoids locking. Borković et al. [36] developed a geometrically exact nonlinear analysis method for elastic curved Euler–Bernoulli beams considering finite but small strain theory.

Within IGA, collocation (IGA-C) methods have been initially introduced as an attempt to address the issue of finding optimal quadrature rules able to fully exploit the high inter-element continuity present in early isogeometric Galerkin (IGA-G) approaches (see, e.g., [37–39]) - even though significant progress has been achieved in, e.g., [39] - yet taking advantage from the higher-order and higher-smoothness of IGA shape functions in terms of, e.g., geometrical flexibility and accuracy. The major advantage of isogeometric collocation over Galerkin-type methods is the minimization of the computational effort with respect to quadrature, since for each degree of freedom, only one point evaluation at a so-called collocation point is required [40]. Also, IGA-C proved to be particularly suitable in the context of structural elements; in particular, it has been successfully applied to study Bernoulli–Euler beams and Kirchhoff plates in [41], while rotation-based Timoshenko beams [42] or mixed formulations both for Timoshenko initially-straight planar [43] and non-prismatic [44] beams, as well as for curved spatial rods [45] have been introduced and studied, and then effectively extended to the geometrically nonlinear case [46–52]. More recent contributions on this theme account for, e.g., multipatch beams [53], viscoelasticity [54], as well as viscoplasticity [55].

While extensive research has been carried out on the static and vibration analysis of IGA curved beams made of isotropic and composite materials, to the best of our knowledge, only a limited number of studies address numerical stress recovery techniques in laminated beams and not in an isogeometric framework. Starting from the work in [56], which takes its origin in e.g., [57–59], Patton et al. introduced a fast and accurate equilibrium-based stress recovery technique to model the out-of-plane behavior of Kirchhoff laminated plates using IGA [60] and immersed IGA [61], extending this approach to study out-of-plane stresses in laminated composite solid plates [62] and shells [63]. This latter post-processing technique has already been proven to provide good results not only in the context of IGA but also of methods based on, e.g., Radial Basis Functions [64]. Vo et al. [65] proposed an isogeometric stress recovery for 2D non-prismatic Timoshenko beams based on the notion of the in-plane stress and stress resultants at the boundary. Balduzzi et al. [66] introduced an enhanced stress recovery for isogeometric Timoshenko beams based on a two-stage iteration process, which ends up with a distribution of stresses that satisfies the first constitutive relation, as well as the horizontal equilibrium partial differential equation. Mercuri et al. [67] derived analytical expressions to recover stresses in non-prismatic finite element beams that are effective for non-trivial geometries and arbitrary load conditions. Recently, Bardella [68] leveraged equilibrium equations to recover through-the-thickness normal stresses in straight sandwich beams subject to linear elastic flexure governed by zigzag warping, where all layers behave according to Timoshenko's kinematics.

The above considerations provide strong motivation to extend the numerical equilibrium-based stress recovery technique proposed, e.g., in [63], to study laminated composite curved beams using IGA. Namely, the stress recovery approach introduced in the present manuscript finds direct application to modeling interlaminar shear stresses in 2D Euler–Bernoulli beams with constant curvature and accounts for bending-stretching coupling, previously neglected in [60], which is in general not negligible for layer arrangements being nonsymmetric about the beam axis. By implementing a systematic reduction of the 3D constitutive model with exact integration throughout the laminate thickness, the proposed framework enhances the overall quality of the stress recovery in the analysis. The proposed approach follows a two-step procedure. Firstly, the Euler–Bernoulli curved beam formulation is solved to obtain the tangent and transverse displacements. Once the displacement solution is computed using either an IGA-G or an IGA-C approach, the normal stress can be directly computed using classical constitutive laws. However, information regarding the transverse stress

state, often associated with delamination, is not readily available. Nevertheless, the interlaminar transverse shear stresses at specific locations of interest can be easily determined by imposing equilibrium equations in strong form in a curvilinear framework. This latter process demands higher-continuity requirements in terms of the displacement solution, which is provided by the IGA shape functions properties. Additionally, given the adopted displacement description along the beam axis, we do not need to transform our solution field from a global to a local system as proposed in [63], which simplifies the stress recovery *a posteriori* step. The paper is structured as follows: Section 2 outlines the governing equations for the planar Euler–Bernoulli composite curved beam with constant curvature posing particular attention on material modeling. In Section 3, we present the fundamentals of univariate NURBS curves, followed by the proposed isogeometric approaches to obtain the approximate displacement field. These displacement-based modeling strategies do not provide an immediate assessment of the transverse stress distributions. However, in Section 4, we describe an equilibrium-based post-processing technique that allows for the recovery of these stress distributions. In Section 5, we conduct various numerical tests to demonstrate the accuracy of the proposed approach. We also examine the behavior of different meshes for increasing length-to-thickness beam ratios and numbers of layers, highlighting the effectiveness of our method. Finally, we present our conclusions in Section 6.

2. General formulation for an Euler–Bernoulli composite curved beam

In this section, we introduce first the kinematic description of Euler–Bernoulli curved beams in curvilinear coordinates. Then, we focus on the material behavior of cross-ply laminated beams considering a systematic reduction of the constitutive relations of the three-dimensional anisotropic body [69] and detail the considered formulation addressing both the weak and strong form level.

2.1. Kinematics

Let us consider the curved beam model in Fig. 1 such that the beam axis passes through the centroid of the (constant) cross-section and is identified by the curvilinear abscissa s, while θ describes the cross section rotation. Analogously, the points of the beam axis can be described in the global reference system X_i ($i = \{1, 2, 3\}$). We assume a longitudinal plane of symmetry (i.e., the beam is planar) which means that the cross-section, constraints, and loading conditions are symmetric to the longitudinal plane. Furthermore, we adopt small strains and Euler–Bernoulli kinematic assumptions (i.e., after deformation, the cross-section remains plane and orthogonal to the deformed beam axis), which allows to neglect the shear strain energy contribution [70]. Also, the beam section is infinitely rigid in its plane, such that there is no deformation in the plane of the cross-section. Therefore, restricting our discussion to structures presenting a constant radius of curvature, $R(s) = \bar{R}$, we introduce the problem variables u and w that describe the displacements along the tangential and normal directions of the curved beam axis, namely along s and z ($z \in [-h/2, h/2]$ being h the thickness of the beam, whereas to complete the description $y \in [-b/2, b/2]$ being b the beam base), respectively.

Under these hypotheses, the only non-zero strain for such an Euler–Bernoulli curved beam can be introduced as

$$\varepsilon_{ss} = \varepsilon^0 - z k^0 , \tag{1}$$

where ε^0 and k^0 indicate the extensional strain and curvature, respectively, of the beam axis (hence the superscript $(.)^0$) and are given as [34,71]:

$$\varepsilon^0 = \frac{\mathrm{d}u}{\mathrm{d}s} + \frac{w}{\bar{R}} , \tag{2a}$$

$$k^0 = -\frac{1}{\bar{R}} \frac{\mathrm{d}u}{\mathrm{d}s} + \frac{\mathrm{d}^2 w}{\mathrm{d}s^2} . \tag{2b}$$

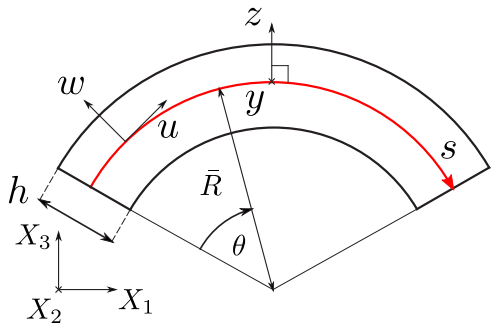

Fig. 1. Geometry of a curved beam depicted in the longitudinal plane of symmetry.

2.2. Constitutive relations

To possibly include the complete stacking sequence contribution in our formulation, we focus on each k-th ply belonging to the laminate and, for ease of description, we will assume that the principal material coordinates coincide with those of the curved beam, namely $\{s, y, z\} = \{x_1, x_2, x_3\}$ (see Fig. 1), which are taken as the composite fiber, matrix, and normal directions. Therefore, the material behavior of each lamina considers three mutually orthogonal planes of material symmetry, allowing to reduce to 9 the number of elastic coefficients of the complete fourth-order elasticity tensor $\mathbb{C}$, such that $\boldsymbol{\sigma} = \mathbb{C} : \boldsymbol{\varepsilon}$, which can be expressed in terms of engineering constants in Voigt's notation as

$$\mathbb{C} = \begin{bmatrix} \mathbb{C}_{11} & \mathbb{C}_{12} & \mathbb{C}_{13} & 0 & 0 & 0 \\ & \mathbb{C}_{22} & \mathbb{C}_{23} & 0 & 0 & 0 \\ & & \mathbb{C}_{33} & 0 & 0 & 0 \\ & \text{symm.} & & \mathbb{C}_{44} & 0 & 0 \\ & & & & \mathbb{C}_{55} & 0 \\ & & & & & \mathbb{C}_{66} \end{bmatrix} = \begin{bmatrix} \frac{1}{E_1} & -\frac{\nu_{12}}{E_1} & -\frac{\nu_{13}}{E_1} & 0 & 0 & 0 \\ & \frac{1}{E_2} & -\frac{\nu_{23}}{E_2} & 0 & 0 & 0 \\ & & \frac{1}{E_3} & 0 & 0 & 0 \\ & \text{symm.} & & \frac{1}{G_{23}} & 0 & 0 \\ & & & & \frac{1}{G_{13}} & 0 \\ & & & & & \frac{1}{G_{12}} \end{bmatrix}^{-1} , \tag{3}$$

where E_1, E_2, and E_3 are the Young's moduli, G_{12}, G_{23}, and G_{13} the shear moduli, and ν_{12}, ν_{23}, and ν_{13} the Poisson's ratios in the principal material coordinates [1].

Then, if the Euler–Bernoulli beam is experiencing only uni-axial bending and no torsional loading, the only relevant stress component is

$$\sigma_{ss} = \mathbb{Q}_{11} \varepsilon_{ss} , \tag{4}$$

where

$$\mathbb{Q}_{11} = \mathbb{C}^*_{11} - \frac{\mathbb{C}^*_{16} \mathbb{C}^*_{16}}{\mathbb{C}^*_{66}} . \tag{5}$$

All $\mathbb{C}^*_{rs}$ ($r, s = \{1, 6\}$) coefficients in Eq. (5) consider a systematic reduction of the constitutive relations of the three-dimensional anisotropic body as in [69] and are taken as

$$\mathbb{C}^*_{11} = \bar{\mathbb{C}}_{11} + \frac{(\bar{\mathbb{C}}_{13}\bar{\mathbb{C}}_{23} - \bar{\mathbb{C}}_{12}\bar{\mathbb{C}}_{33})}{(\bar{\mathbb{C}}_{22}\bar{\mathbb{C}}_{33} - \bar{\mathbb{C}}_{23}\bar{\mathbb{C}}_{23})} \bar{\mathbb{C}}_{12} + \frac{(\bar{\mathbb{C}}_{12}\bar{\mathbb{C}}_{23} - \bar{\mathbb{C}}_{13}\bar{\mathbb{C}}_{22})}{(\bar{\mathbb{C}}_{22}\bar{\mathbb{C}}_{33} - \bar{\mathbb{C}}_{23}\bar{\mathbb{C}}_{23})} \bar{\mathbb{C}}_{13} , \tag{6a}$$

$$\mathbb{C}^*_{16} = \bar{\mathbb{C}}_{16} + \frac{(\bar{\mathbb{C}}_{36}\bar{\mathbb{C}}_{23} - \bar{\mathbb{C}}_{26}\bar{\mathbb{C}}_{33})}{(\bar{\mathbb{C}}_{22}\bar{\mathbb{C}}_{33} - \bar{\mathbb{C}}_{23}\bar{\mathbb{C}}_{23})} \bar{\mathbb{C}}_{12} + \frac{(\bar{\mathbb{C}}_{26}\bar{\mathbb{C}}_{23} - \bar{\mathbb{C}}_{36}\bar{\mathbb{C}}_{22})}{(\bar{\mathbb{C}}_{22}\bar{\mathbb{C}}_{33} - \bar{\mathbb{C}}_{23}\bar{\mathbb{C}}_{23})} \bar{\mathbb{C}}_{13} , \tag{6b}$$

$$\mathbb{C}^{*}_{66} = \bar{\mathbb{C}}_{66} + \frac{\left(\bar{\mathbb{C}}_{36}\bar{\mathbb{C}}_{23} - \bar{\mathbb{C}}_{26}\bar{\mathbb{C}}_{33}\right)}{\left(\bar{\mathbb{C}}_{22}\bar{\mathbb{C}}_{33} - \bar{\mathbb{C}}_{23}\bar{\mathbb{C}}_{23}\right)}\bar{\mathbb{C}}_{26} + \frac{\left(\bar{\mathbb{C}}_{26}\bar{\mathbb{C}}_{23} - \bar{\mathbb{C}}_{36}\bar{\mathbb{C}}_{22}\right)}{\left(\bar{\mathbb{C}}_{22}\bar{\mathbb{C}}_{33} - \bar{\mathbb{C}}_{23}\bar{\mathbb{C}}_{23}\right)}\bar{\mathbb{C}}_{36}\,, \tag{6c}$$

where $\bar{\mathbb{C}}_{ab}$ $(a,b=\{1,2,3,6\})$ are the components of the IV-order elasticity tensor (3) for a fiber-reinforced composite lamina whose tangential (principal) material axis is oriented at an angle α with respect to the x_1-axis and can be detailed as

$$\bar{\mathbb{C}}_{11} = \mathbb{C}_{11}\cos\alpha^4 + 2\left(\mathbb{C}_{12}+2\mathbb{C}_{66}\right)\sin\alpha^2\cos\alpha^2 + \mathbb{C}_{22}\sin\alpha^4\,, \tag{7a}$$

$$\bar{\mathbb{C}}_{12} = \left(\mathbb{C}_{11}+\mathbb{C}_{22}-4\mathbb{C}_{66}\right)\sin\alpha^2\cos\alpha^2 + \mathbb{C}_{12}\left(\sin\alpha^4+\cos\alpha^4\right)\,, \tag{7b}$$

$$\bar{\mathbb{C}}_{13} = \mathbb{C}_{13}\cos\alpha^2 + \mathbb{C}_{23}\sin\alpha^2\,, \tag{7c}$$

$$\bar{\mathbb{C}}_{16} = \left(\mathbb{C}_{11}-\mathbb{C}_{12}-2\mathbb{C}_{66}\right)\sin\alpha\cos\alpha^3 + \left(\mathbb{C}_{12}-\mathbb{C}_{22}+2\mathbb{C}_{66}\right)\sin\alpha^3\cos\alpha\,, \tag{7d}$$

$$\bar{\mathbb{C}}_{22} = \mathbb{C}_{11}\sin\alpha^4 + 2\left(\mathbb{C}_{12}+2\mathbb{C}_{66}\right)\sin\alpha^2\cos\alpha^2 + \mathbb{C}_{22}\cos\alpha^4\,, \tag{7e}$$

$$\bar{\mathbb{C}}_{23} = \mathbb{C}_{13}\sin\alpha^2 + \mathbb{C}_{23}\cos\alpha^2\,, \tag{7f}$$

$$\bar{\mathbb{C}}_{26} = \left(\mathbb{C}_{11}-\mathbb{C}_{12}-2\mathbb{C}_{66}\right)\sin\alpha^3\cos\alpha + \left(\mathbb{C}_{12}-\mathbb{C}_{22}+2\mathbb{C}_{66}\right)\sin\alpha\cos\alpha^3\,, \tag{7g}$$

$$\bar{\mathbb{C}}_{33} = \mathbb{C}_{33}\,, \tag{7h}$$

$$\bar{\mathbb{C}}_{36} = \left(\mathbb{C}_{13}-\mathbb{C}_{23}\right)\cos\alpha\sin\alpha\,, \tag{7i}$$

$$\bar{\mathbb{C}}_{66} = \left(\mathbb{C}_{11}+\mathbb{C}_{22}-2\mathbb{C}_{12}-2\mathbb{C}_{66}\right)\sin\alpha^2\cos\alpha^2 + \mathbb{C}_{66}\left(\sin\alpha^4+\cos\alpha^4\right)\,. \tag{7j}$$

At this point, we can classically introduce the in-plane force N and moment M resultants as

$$N = \int_A \sigma_{ss}\,dA\,, \tag{8a}$$

$$M = \int_A z\sigma_{ss}\,dA\,, \tag{8b}$$

which, once substituting Eq. (4) and integrating through the beam cross-section, can be expressed as

$$\begin{pmatrix} N \\ M \end{pmatrix} = \begin{bmatrix} A & B \\ B & D \end{bmatrix}\begin{pmatrix} \varepsilon^0 \\ -k^0 \end{pmatrix}\,, \tag{9}$$

where A, B, and D are calculated as:

$$(A,B,D) = b\int_{-h/2}^{h/2}\bar{Q}^k_{11}\left(1,z,z^2\right)\mathrm{d}z\,. \tag{10}$$

2.3. Principle of virtual works

We consider Hamilton's principle in order to derive the governing equation weak form:

$$\int_0^{\bar{s}}\delta\left(U-V\right)\mathrm{d}s = 0\,, \tag{11}$$

where U and V are the strain energy and external work, respectively. The virtual strain energy can be then calculated as:

$$\delta U = \int_0^{\bar{s}}\left(N\delta\varepsilon^0 - M\delta k^0\right)\mathrm{d}s\,, \tag{12}$$

and further detailed by substituting Eqs. (2):

$$\begin{aligned}\delta U &= \int_0^{\bar{s}}\left(N\delta\left(\frac{\mathrm{d}u}{\mathrm{d}s}+\frac{w}{\bar{R}}\right) - M\delta\left(-\frac{1}{\bar{R}}\frac{\mathrm{d}u}{\mathrm{d}s}+\frac{\mathrm{d}^2w}{\mathrm{d}s^2}\right)\right)\mathrm{d}s \\ &= \int_0^{\bar{s}}\left(N\left(\frac{\mathrm{d}\delta u}{\mathrm{d}s}+\frac{\delta w}{\bar{R}}\right) - M\left(-\frac{1}{\bar{R}}\frac{\mathrm{d}\delta u}{\mathrm{d}s}+\frac{\mathrm{d}^2\delta w}{\mathrm{d}s^2}\right)\right)\mathrm{d}s\,.\end{aligned} \tag{13}$$

Then, by inserting Eqs. (8) into Eq. (13), once expressed in terms of membrane strain and curvature (see Eqs. (2)), we obtain a displacement-based expression of δU:

$$\begin{aligned}\delta U = \int_0^{\bar{s}}\Bigg(& A\left(\frac{\mathrm{d}u}{\mathrm{d}s}\frac{\mathrm{d}\delta u}{\mathrm{d}s}+\frac{\mathrm{d}u}{\mathrm{d}s}\frac{\delta w}{\bar{R}}+\frac{w}{\bar{R}}\frac{\mathrm{d}\delta u}{\mathrm{d}s}+\frac{1}{\bar{R}^2}w\delta w\right) \\ & - B\left(-\frac{1}{\bar{R}}\frac{\mathrm{d}u}{\mathrm{d}s}\frac{\mathrm{d}\delta u}{\mathrm{d}s}+\frac{\mathrm{d}^2w}{ds^2}\frac{\mathrm{d}\delta u}{\mathrm{d}s}-\frac{1}{\bar{R}^2}\frac{\mathrm{d}u}{\mathrm{d}s}\delta w+\frac{\mathrm{d}^2w}{ds^2}\frac{\delta w}{\bar{R}}\right) \\ & - B\left(-\frac{1}{\bar{R}}\frac{\mathrm{d}u}{\mathrm{d}s}\frac{\mathrm{d}\delta u}{\mathrm{d}s}+\frac{\mathrm{d}u}{\mathrm{d}s}\frac{\mathrm{d}^2\delta w}{ds^2}-\frac{w}{\bar{R}^2}\frac{\mathrm{d}\delta u}{\mathrm{d}s}+\frac{w}{\bar{R}}\frac{\mathrm{d}^2\delta w}{ds^2}\right) \\ & + D\left(\frac{1}{\bar{R}^2}\frac{\mathrm{d}u}{\mathrm{d}s}\frac{\mathrm{d}\delta u}{\mathrm{d}s}-\frac{1}{\bar{R}}\frac{\mathrm{d}u}{\mathrm{d}s}\frac{\mathrm{d}^2\delta w}{ds^2}-\frac{1}{\bar{R}}\frac{\mathrm{d}\delta u}{\mathrm{d}s}\frac{\mathrm{d}^2w}{ds^2}+\frac{\mathrm{d}^2w}{ds^2}\frac{\mathrm{d}^2\delta w}{ds^2}\right)\Bigg)\mathrm{d}s \\ = \int_0^{\bar{s}}\Bigg(& \left(A+\frac{2B}{\bar{R}}+\frac{D}{\bar{R}^2}\right)\frac{\mathrm{d}u}{\mathrm{d}s}\frac{\mathrm{d}\delta u}{\mathrm{d}s} \\ & + \left(\left(\frac{A}{\bar{R}}+\frac{B}{\bar{R}^2}\right)\frac{\mathrm{d}u}{\mathrm{d}s}\delta w - \left(B+\frac{D}{\bar{R}}\right)\frac{\mathrm{d}u}{\mathrm{d}s}\frac{\mathrm{d}^2\delta w}{ds^2}\right) \\ & + \left(\left(\frac{A}{\bar{R}}+\frac{B}{\bar{R}^2}\right)w\frac{\mathrm{d}\delta u}{\mathrm{d}s} - \left(B+\frac{D}{\bar{R}}\right)\frac{\mathrm{d}^2w}{ds^2}\frac{\mathrm{d}\delta u}{\mathrm{d}s}\right) \\ & + \left(\frac{A}{\bar{R}^2}w\delta w - \frac{B}{\bar{R}}\frac{\mathrm{d}^2w}{ds^2}\delta w - \frac{B}{\bar{R}}w\frac{\mathrm{d}^2\delta w}{ds^2} + D\frac{\mathrm{d}^2w}{ds^2}\frac{\mathrm{d}^2\delta w}{ds^2}\right)\Bigg)\mathrm{d}s\,.\end{aligned} \tag{14}$$

Finally, the external virtual work can be written as:

$$\delta V = \int_0^{\bar{s}}\left(p_u\delta u + p_w\delta w\right)\mathrm{d}s + \left(P_u\bar{u}\right)\Big|_0^{\bar{s}} + \left(P_w\bar{w}\right)\Big|_0^{\bar{s}} + \left(\bar{M}\bar{\phi}\right)\Big|_0^{\bar{s}}\,, \tag{15}$$

where p_u and p_w are the distributed load per unit of beam axis length along s and z directions (see Fig. 1), P_u, P_w, and $\bar{M}$ are the tangential force, the transverse force, and the moment, while $\bar{u}$, $\bar{w}$, and $\bar{\phi}$ are the generalized displacements possibly applied at the boundary of the beam.

2.4. Strong form

Integrating Eq. (13) by parts yields:

$$\begin{aligned}&\int_0^{\bar{s}}\left(-\frac{\mathrm{d}N}{\mathrm{d}s}-\frac{1}{\bar{R}}\frac{\mathrm{d}M}{\mathrm{d}s}-P_u\right)\delta u\,\mathrm{d}s + \int_0^{\bar{s}}\left(\frac{N}{\bar{R}}-\frac{\mathrm{d}^2M}{\mathrm{d}s^2}-P_w\right)\delta w\,\mathrm{d}s \\ &+ \left(N\delta u\right)\Big|_0^{\bar{s}} + \left(M\left(\frac{\delta u}{\bar{R}}-\frac{\mathrm{d}\delta w}{\mathrm{d}s}\right)\right)\Big|_0^{\bar{s}} + \left(\frac{\mathrm{d}M}{\mathrm{d}s}\delta w\right)\Big|_0^{\bar{s}} = 0\,.\end{aligned} \tag{16}$$

Then, we introduce the problem domain as $\Omega = (0,\bar{s})$ and its boundary by $\Gamma = \{0\}\cup\{\bar{s}\}$ such that Γ can be decomposed as $\Gamma = \Gamma_u\cup\Gamma_N$, $\Gamma = \Gamma_w\cup\Gamma_V$, and $\Gamma = \Gamma_\phi\cup\Gamma_M$ with $\Gamma_u\cap\Gamma_N = \emptyset$, $\Gamma_w\cap\Gamma_V = \emptyset$, $\Gamma_\phi\cap\Gamma_M = \emptyset$. Following [41], to ensure the well-posedness of the problem, we require that $\Gamma_w\neq\emptyset$, while Γ_ϕ, Γ_N, Γ_V, and Γ_M are allowed to be empty sets. Given the distributed tangential and transverse loads $p_u, p_w : \Omega\to\mathbb{R}$ and the boundary condition functions, namely the tangential $\bar{u} : \Gamma_u\to\mathbb{R}$ and transverse displacement $\bar{w} : \Gamma_w\to\mathbb{R}$, rotation $\bar{\phi} : \Gamma_\phi\to\mathbb{R}$, as well as $P_u : \Gamma_u\to\mathbb{R}$, $P_w : \Gamma_w\to\mathbb{R}$, and $\bar{M} : \Gamma_\phi\to\mathbb{R}$, we can introduce the boundary value problem [1] associated with an elastic Euler–Bernoulli beam, as Eq. (16) holds for every δu and δw:

$$\frac{\mathrm{d}N}{\mathrm{d}s}+\frac{1}{\bar{R}}\frac{\mathrm{d}M}{\mathrm{d}s}+p_u = 0 \quad \text{in } \Omega\,, \tag{17a}$$

$$\frac{N}{\bar{R}}-\frac{\mathrm{d}^2M}{\mathrm{d}s^2}-p_w = 0 \quad \text{in } \Omega\,, \tag{17b}$$

$$u = \bar{u} \quad \text{on } \Gamma_u\,, \tag{17c}$$

$$w = \bar{w} \quad \text{on } \Gamma_w\,, \tag{17d}$$

$$\frac{u}{\bar{R}}-\frac{\mathrm{d}w}{\mathrm{d}s} = \bar{\phi} \quad \text{on } \Gamma_\phi\,, \tag{17e}$$

[1] To avoid redundancy in the inter-text flow, we choose not to express Eq. (17g) in terms of displacements, as it can be easily obtained by taking the derivative of Eq. (18b) with respect to s.

$$N = P_u \qquad \text{on } \Gamma_N\,, \tag{17f}$$

$$\frac{\mathrm{d}M}{\mathrm{d}s} = P_w \qquad \text{on } \Gamma_V\,, \tag{17g}$$

$$M = \bar{M} \qquad \text{on } \Gamma_M\,. \tag{17h}$$

Then, inserting Eqs. (2) into (9), we can further detail the in-plane force and moment resultants as

$$N = \left(\left(A + \frac{B}{\bar{R}}\right)\frac{\mathrm{d}u}{\mathrm{d}s} + A\frac{w}{\bar{R}} - B\frac{\mathrm{d}^2 w}{\mathrm{d}s^2}\right), \tag{18a}$$

$$M = \left(\left(B + \frac{D}{\bar{R}}\right)\frac{\mathrm{d}u}{\mathrm{d}s} + B\frac{w}{\bar{R}} - D\frac{\mathrm{d}^2 w}{\mathrm{d}s^2}\right), \tag{18b}$$

and rewrite Euler–Lagrange Eqs. (17a) and (17b) in terms of displacements as follows:

$$\left(A + \frac{2B}{\bar{R}} + \frac{D}{\bar{R}^2}\right)\frac{\mathrm{d}^2 u}{\mathrm{d}s^2} + \frac{1}{\bar{R}}\left(A + \frac{B}{\bar{R}}\right)\frac{\mathrm{d}w}{\mathrm{d}s} - \left(B + \frac{D}{\bar{R}}\right)\frac{\mathrm{d}^3 w}{\mathrm{d}s^3} + p_u = 0\,, \tag{19a}$$

$$\frac{1}{\bar{R}}\left(A + \frac{B}{\bar{R}}\right)\frac{\mathrm{d}u}{\mathrm{d}s}\left(B + \frac{D}{\bar{R}}\right)\frac{\mathrm{d}^3 u}{\mathrm{d}s^3} + \frac{A}{\bar{R}^2}w - \frac{2B}{\bar{R}}\frac{\mathrm{d}^2 w}{\mathrm{d}s^2} + D\frac{\mathrm{d}^4 w}{\mathrm{d}s^4} - p_w = 0\,. \tag{19b}$$

3. Isogeometric strategies for laminated planar Euler–Bernoulli curved beams

In this section, we recall the notions of univariate NURBS curves and detail the investigated numerical isogeometric approaches, namely a classical Galerkin method and a collocation approach, to approximate Euler–Bernoulli laminated beams.

3.1. Univariate NURBS curves

Since the geometry of the curved beam axis is described by a NURBS curve, we proceed to briefly revise basic notions of univariate B-splines and NURBS, while, for a more comprehensive discussion, readers may refer to [29,72] and references therein.

To describe univariate B-spline basis functions of fixed order p (i.e., the polynomial degree), we recall the so-called "knot vector" definition, that is in one dimension a non-decreasing set of coordinates in the parameter space $\hat{\Omega}$:

$$\Xi = \left[\xi_1, \xi_2, \ldots, \xi_i, \ldots, \xi_{m+p+1}\right]\,, \tag{20}$$

where $\xi_i \in \mathbb{R}$ is the i-th knot, i is the knot index ($i = \{1, 2, \ldots, m+p+1\}$), and m is the associated number of basis functions. Then, univariate B-spline basis functions can be defined recursively *via* the Cox-de Boor formula [73], starting from piecewise constants ($p = 0$):

$$B_{i,0}(\xi) = \begin{cases} 1 \;\; if \;\; \xi_i \le \xi < \xi_{i+1} \\ 0 \;\; \text{otherwise} \end{cases}\,, \tag{21}$$

while for $p = 1, 2, 3, \ldots$, they are constructed as

$$B_{i,p}(\xi) = \frac{\xi - \xi_i}{\xi_{i+p} - \xi_i}B_{i,p-1}(\xi) + \frac{\xi_{i+p+1} - \xi}{\xi_{i+p+1} - \xi_{i+1}}B_{i+1,p-1}(\xi)\,, \tag{22}$$

where the convention $0/0 = 0$ is assumed. Thus, univariate NURBS basis functions of order p can be defined as the projection onto a d_s-dimensional physical space of non-rational (polynomial) B-splines defined in a d_s+1-dimensional homogeneous coordinate space and read

$$R_i^p(\xi) = \frac{B_{i,p}w_i}{\sum_{\bar{i}=1}^{n_{cp}} B_{\bar{i},p}(\xi)w_{\bar{i}}}\,, \tag{23}$$

where w_i represents the NURBS weight associated to each i-th control point and consists of its $d_s + 1$-component in the homogeneous space.

NURBS curves are then introduced by taking a linear combination of univariate NURBS basis functions and control points as

$$\mathbf{C}(\xi) = \sum_{j=1}^{m} R_i^p(\xi)\,\mathbf{P}_i\,. \tag{24}$$

3.2. IGA Galerkin approach

Once the geometry of the curved beam axis is described by a NURBS curve, adopting the isoparametric concept, the tangential and transverse displacements are approximated by a linear combination of NURBS functions $\left\{R_1^p, R_2^p, \ldots, R_i^p \ldots, R_m^p\right\}$ and unknown control variables $\left\{\hat{u}_1, \hat{u}_2, \ldots, \hat{u}_i, \ldots, \hat{u}_m\right\}$ and $\left\{\hat{w}_1, \hat{w}_2, \ldots, \hat{w}_i, \ldots, \hat{w}_m\right\}$ as follows:

$$u \approx u_h = \sum_{i=1}^{m} R_i^p \hat{u}_i\,, \tag{25a}$$

$$w \approx w_h = \sum_{i=1}^{m} R_i^p \hat{w}_i\,. \tag{25b}$$

Then, to obtain the discrete weak form of the internal and external virtual work in primal form (neglecting with no loss of generality generalized point loads), we substitute in relations (14) and (15) the primal fields expressed by Eqs. (25) as well as the discretized counterpart of virtual displacements, δu and δw, which are approximated by the same functions used for the displacement field approximation (25). Therefore, addressing the element point of view, the control variables spanning over each element e can be rearranged into the tangential $\hat{\boldsymbol{u}}^e = [\hat{u}_1^e, \hat{u}_2^e, \ldots, \hat{u}_{\text{nen}}^e]$ and transverse $\hat{\boldsymbol{w}}^e = [\hat{w}_1^e, \hat{w}_2^e, \ldots, \hat{w}_{\text{nen}}^e]$ displacement element vectors (being nen the total local number of control variables), leading to:

$$\delta U \approx \sum_{e=1}^{\text{nel}} \delta U^e = \sum_{e=1}^{\text{nel}} \begin{pmatrix} \delta\hat{\boldsymbol{u}}^e & \delta\hat{\boldsymbol{w}}^e \end{pmatrix} \begin{bmatrix} \boldsymbol{K}_{uu}^e & \boldsymbol{K}_{uw}^e \\ \boldsymbol{K}_{wu}^e & \boldsymbol{K}_{ww}^e \end{bmatrix} \begin{pmatrix} \hat{\boldsymbol{u}}^e \\ \hat{\boldsymbol{w}}^e \end{pmatrix}\,, \tag{26a}$$

$$\delta V \approx \sum_{e=1}^{\text{nel}} \delta V^e = \sum_{e=1}^{\text{nel}} \begin{pmatrix} \delta\hat{\boldsymbol{u}}^e & \delta\hat{\boldsymbol{w}}^e \end{pmatrix} \begin{pmatrix} \boldsymbol{F}_u^e \\ \boldsymbol{F}_w^e \end{pmatrix}\,, \tag{26b}$$

where the element stiffness matrix and force vector sub-blocks are defined as:

$$\boldsymbol{K}_{uu}^e = \int_0^{\bar{s}} \sum_{\hat{i}=1}^{\text{nen}} \sum_{\hat{j}=1}^{\text{nen}} \left(\left(A + \frac{2B}{\bar{R}} + \frac{D}{\bar{R}^2}\right)\frac{\mathrm{d}R_{\hat{i}}^p}{\mathrm{d}s}\frac{\mathrm{d}R_{\hat{j}}^p}{\mathrm{d}s}\right)\mathrm{d}s\,, \tag{27a}$$

$$\boldsymbol{K}_{uw}^e = \int_0^{\bar{s}} \sum_{\hat{i}=1}^{\text{nen}} \sum_{\hat{j}=1}^{\text{nen}} \left(\left(\frac{A}{\bar{R}} + \frac{B}{\bar{R}^2}\right)\frac{\mathrm{d}R_{\hat{i}}^p}{\mathrm{d}s}R_{\hat{j}}^p - \left(B + \frac{D}{\bar{R}}\right)\frac{\mathrm{d}^2 R_{\hat{i}}^p}{\mathrm{d}s^2}\frac{\mathrm{d}^2 R_{\hat{j}}^p}{\mathrm{d}s^2}\right)\mathrm{d}s\,, \tag{27b}$$

$$\boldsymbol{K}_{wu}^e = \left(\boldsymbol{K}_{uw}^e\right)^{\mathrm{T}}\,, \tag{27c}$$

$$\boldsymbol{K}_{ww}^e = \int_0^{\bar{s}} \sum_{\hat{i}=1}^{\text{nen}} \sum_{\hat{j}=1}^{\text{nen}} \Big(\frac{A}{\bar{R}^2}R_{\hat{i}}^p R_{\hat{j}}^p - \frac{B}{\bar{R}}\frac{\mathrm{d}^2 R_{\hat{i}}^p}{\mathrm{d}s^2}R_{\hat{j}}^p - \frac{B}{\bar{R}}R_{\hat{i}}^p\frac{\mathrm{d}^2 R_{\hat{j}}^p}{\mathrm{d}s^2} + D\frac{\mathrm{d}^2 R_{\hat{i}}^p}{\mathrm{d}s^2}\frac{\mathrm{d}^2 R_{\hat{j}}^p}{\mathrm{d}s^2}\Big)\mathrm{d}s\,, \tag{27d}$$

$$\boldsymbol{F}_u^e = \int_0^{\bar{s}} \sum_{\hat{i}=1}^{\text{nen}} \left(R_{\hat{i}}^p p_u\right)\mathrm{d}s\,, \tag{27e}$$

$$\boldsymbol{F}_w^e = \int_0^{\bar{s}} \sum_{\hat{i}=1}^{\text{nen}} \left(R_{\hat{i}}^p p_w\right)\mathrm{d}s\,. \tag{27f}$$

Here, in order to integrate Eqs. (26), we have to compute the Jacobian of the transformation between coordinates $s = R\theta$ and ξ, as well as the

radius of curvature [34], which are given by:

$$J = \frac{\mathrm{d}(R\theta)}{\mathrm{d}\xi} = \frac{\mathrm{d}s}{\mathrm{d}\xi} = \sqrt{\left(\frac{\mathrm{d}X_1}{\mathrm{d}\xi}\right)^2 + \left(\frac{\mathrm{d}X_3}{\mathrm{d}\xi}\right)^2}, \tag{28a}$$

$$R(s) = \frac{J^3}{\left|\frac{\mathrm{d}X_1}{\mathrm{d}\xi}\frac{\mathrm{d}^2X_3}{\mathrm{d}\xi^2} - \frac{\mathrm{d}X_3}{\mathrm{d}\xi}\frac{\mathrm{d}^2X_1}{\mathrm{d}\xi^2}\right|}, \tag{28b}$$

where $X_1(\xi)$ and $X_3(\xi)$ are the global coordinates that describe the curve (see Fig. 1). Moreover, we need to detail the first, second, and third derivatives of the i-th shape function R_i^p with respect to s, which read:

$$\frac{\mathrm{d}R_i^p}{\mathrm{d}s} = \frac{\mathrm{d}R_i^p}{\mathrm{d}\xi}\frac{\mathrm{d}\xi}{\mathrm{d}s}, \tag{29a}$$

$$\frac{\mathrm{d}^2R_i^p}{\mathrm{d}s^2} = \frac{1}{\left(\frac{\mathrm{d}s}{\mathrm{d}\xi}\right)^2}\left(\frac{\mathrm{d}^2R_i^p}{\mathrm{d}\xi^2} - \frac{\mathrm{d}R_i^p}{\mathrm{d}s}\frac{\mathrm{d}^2s}{\mathrm{d}\xi^2}\right), \tag{29b}$$

$$\frac{\mathrm{d}^3R_i^p}{\mathrm{d}s^3} = \frac{1}{\left(\frac{\mathrm{d}s}{\mathrm{d}\xi}\right)^3}\left[\frac{\mathrm{d}^3R_i^p}{\mathrm{d}\xi^3} - \left(2\frac{\mathrm{d}^2R_i^p}{\mathrm{d}s^2}\frac{\mathrm{d}s}{\mathrm{d}\xi}\frac{\mathrm{d}^2s}{\mathrm{d}\xi^2} + \frac{\mathrm{d}^2R_i^p}{\mathrm{d}s^2}\frac{\mathrm{d}^3s}{\mathrm{d}\xi^3} + \frac{\mathrm{d}R_i^p}{\mathrm{d}s}\frac{\mathrm{d}^3s}{\mathrm{d}\xi^3}\right)\right]. \tag{29c}$$

Remark 1. We highlight that to integrate the element stiffness sub-blocks in Eqs. (27), we utilize a standard quadrature rule which comprises $p+1$ points per element.

3.3. IGA collocation approach

Collocation strategies (see, e.g., [40,74,75] for further details) directly discretize the strong form of the set of partial differential equations governing the problem, which are evaluated at the so-called "collocation points". In this work, we adopt the simplest and most widespread approach in the engineering literature, and we collocate the governing strong-form equations at the images of "Greville abscissae" (see, e.g., [76]). For alternative choices of collocation points, the interested reader is referred to e.g., [77]. Greville abscissae consist of a set of n points along the parametric direction ξ, obtained from the knot vector components, ξ_i, as

$$\tau_k = \frac{\xi_{k+1} + \xi_{k+2} + \cdots + \xi_{k+p}}{p} \qquad k = 1, 2, \dots, n, \tag{30}$$

where p is the polynomial order. As for an IGA Galerkin approach, also within an IGA collocation method, problem variables are approximated as linear combinations of IGA basis functions and control variables (see Eq. (25)). Without loss of generality, we will focus on the discretization of a clamped beam subjected to a point load at the free edge, which will be of aid to the numerical test section. Other boundary conditions are, of course, possible and may be easily considered. Following [41], we will use an open knot vector such that $\tau_1 = \xi_1 = 0$ and $\tau_n = \xi_{m+p+1} = \bar{s}$ and assume $p \geq 4$ to fulfill the minimum regularity requirement to collocate Eqs. (19). Our strong form problem (see Eqs. (17)) features in Ω a coupled system of differential equations comprising a second-order operator in u and a fourth-order one in w. Therefore, to obtain a well-posed boundary-value problem for a second-order differential equation, we need to impose one boundary condition at each boundary point, whereas we need to impose two for the fourth-order differential equation. Therefore, our collocation strategy for the problem under consideration is as follows:

$$\begin{cases}
u_h(\tau_1) = 0, & \text{(a)}\\
\left(A + \frac{2B}{\bar{R}} + \frac{D}{\bar{R}^2}\right)\frac{\mathrm{d}^2u_h(\tau_k)}{\mathrm{d}s^2} + \frac{1}{\bar{R}}\left(A + \frac{B}{\bar{R}}\right)\frac{\mathrm{d}w_h(\tau_k)}{\mathrm{d}s} - \left(B + \frac{D}{\bar{R}}\right)\frac{\mathrm{d}^3w_h(\tau_k)}{\mathrm{d}s^3} = 0 \qquad k = 3, 4, \dots, n-2, & \text{(b)}\\
\left(A + \frac{B}{\bar{R}}\right)\frac{\mathrm{d}u_h(\tau_n)}{\mathrm{d}s} + \frac{A}{\bar{R}}w_h(\tau_n) - B\frac{\mathrm{d}^2w_h(\tau_n)}{\mathrm{d}s^2} = 0, & \text{(c)}\\
w_h(\tau_1) = 0, & \text{(d)}\\
\frac{u_h(\tau_1)}{\bar{R}} - \frac{\mathrm{d}w_h(\tau_1)}{\mathrm{d}s} = 0, & \text{(e)}\\
\frac{1}{\bar{R}}\left(A + \frac{B}{\bar{R}}\right)\frac{\mathrm{d}u_h(\tau_k)}{\mathrm{d}s} - \left(B + \frac{D}{\bar{R}}\right)\frac{\mathrm{d}^3u_h(\tau_k)}{\mathrm{d}s^3} + \frac{A}{\bar{R}^2}w_h(\tau_k) - \frac{2B}{\bar{R}}\frac{\mathrm{d}^2w_h(\tau_k)}{\mathrm{d}s^2} + D\frac{\mathrm{d}^4w_h(\tau_k)}{\mathrm{d}s^4} = 0 \qquad k = 2, 4, \dots, n-1, & \text{(f)}\\
\left(B + \frac{D}{\bar{R}}\right)\frac{\mathrm{d}^2u_h(\tau_n)}{\mathrm{d}s^2} + \frac{B}{\bar{R}}\frac{\mathrm{d}w_h(\tau_n)}{\mathrm{d}s} - D\frac{\mathrm{d}^3w_h(\tau_n)}{\mathrm{d}s^3} = P_w, & \text{(g)}\\
\left(B + \frac{D}{\bar{R}}\right)\frac{\mathrm{d}u_h(\tau_n)}{\mathrm{d}s} + \frac{B}{\bar{R}}w_h(\tau_n) - D\frac{\mathrm{d}^2w_h(\tau_n)}{\mathrm{d}s^2} = 0. & \text{(h)}
\end{cases} \tag{31}$$

To completely clamp $\xi_1 = 0$, we impose that the control variables for the first collocation point are zero, namely, $\hat{u}_1 = 0$ (as in Eq. (31a)) and $\hat{w}_1 = 0$ (see Eq. (31d)), whereas we set a zero rotation at τ_1, collocating Eq. (31e). To apply instead a transverse point load at the free edge $\xi_{m+p+1} = \bar{s}$, together with a zero in-plane force and moment, we will collocate Eqs. (31g), (31c), and (31h), respectively. As we can rely on $2n$ equations and we need to impose 6 boundary conditions overall, we will utilize $(n-2) + (n-4) + 6$ relations (namely, $(n-2) + (n-4)$ to collocate the internal body Eqs. (31b) and (31f) plus the 6 boundary conditions) and disregard to collocate Eq. (31b) for collocation point τ_2 and τ_{n-1}. The final system to solve reads (see Eqs. (32) in Box I), where we recall that m is the total number of shape functions R_i^p. Collocating Eq. (32c), we need to utilize relations (29) together with the fourth-order derivative of the i-th shape function R_i^p with respect to s which we compute by means of the chain rule:

$$\frac{\mathrm{d}^4R_i^p}{\mathrm{d}s^4} = \frac{1}{\left(\frac{\mathrm{d}s}{\mathrm{d}\xi}\right)^4}\left\{\frac{\mathrm{d}^4R_i^p}{\mathrm{d}\xi^4} - \left[6\frac{\mathrm{d}^3R_i^p}{\mathrm{d}s^3}\left(\frac{\mathrm{d}s}{\mathrm{d}\xi}\right)^2\frac{\mathrm{d}^2s}{\mathrm{d}\xi^2} + \frac{\mathrm{d}^2R_i^p}{\mathrm{d}s^2}\left(4\frac{\mathrm{d}s}{\mathrm{d}\xi}\frac{\mathrm{d}^3s}{\mathrm{d}\xi^3} + 3\left(\frac{\mathrm{d}^2s}{\mathrm{d}\xi^2}\right)^2\right) + \frac{\mathrm{d}R_i^p}{\mathrm{d}s}\frac{\mathrm{d}^4s}{\mathrm{d}\xi^4}\right]\right\}. \tag{33}$$

4. Local stress recovery for laminated Euler–Bernoulli curved beams

In this section, we adapt the stress recovery technique introduced in [63] for curved structures to Euler–Bernoulli curved beams and study the transverse shear stress distribution through the laminate thickness. Given the adopted displacement description along the beam axis, we do not need to transform our solution field from a global to a local system as proposed in [63], which leads to an even more direct and straightforward stress recovery. Therefore, the equilibrium equation can be written with respect to the curvilinear system as:

$$\left(z + \bar{R}\right)\bar{R}\sigma_{ss,s} + \left(\left(z + \bar{R}\right)^2\sigma_{sz}\right)_{,z} + b_s = 0, \tag{34}$$

being b_s the tangential force per unit of beam volume. In Eq. (34), σ_{ss} is already the normal stress component that is well approximated starting from the obtained displacement field (u, w), whereas σ_{sz} is the transverse shear stress, which cannot be directly assessed in this type of formulation using constitutive equations. However, relying on IGA shape functions high-order continuity properties, we are able to accurately approximate also the derivatives of normal stresses $\sigma_{ss,s}$, thereby recovering the transverse shear integrating along the beam

$$
\begin{cases}
\displaystyle\sum_{i=1}^{m}\begin{bmatrix} R_i^p(\tau_1) & 0 \\ 0 & R_i^p(\tau_1)\end{bmatrix}\cdot\begin{pmatrix}\hat{u}_i\\ \hat{w}_i\end{pmatrix}=\begin{pmatrix}0\\0\end{pmatrix}, & \text{(a)}\\
\displaystyle\sum_{i=1}^{m}\begin{bmatrix}\frac{R_i^p(\tau_1)}{\bar{R}} & -\frac{\mathrm{d}R_i^p(\tau_1)}{\mathrm{d}s}\end{bmatrix}\cdot\begin{pmatrix}\hat{u}_i\\ \hat{w}_i\end{pmatrix}=0, & \text{(b)}\\
\displaystyle\sum_{i=1}^{m}\begin{bmatrix} \left(A+\frac{2B}{\bar{R}}+\frac{D}{\bar{R}^2}\right)\frac{\mathrm{d}^2R_i^p(\tau_j)}{\mathrm{d}s^2} & \frac{1}{\bar{R}}\left(A+\frac{B}{\bar{R}}\right)\frac{\mathrm{d}R_i^p(\tau_j)}{\mathrm{d}s}-\left(B+\frac{D}{\bar{R}}\right)\frac{\mathrm{d}^3R_i^p(\tau_j)}{\mathrm{d}s^3}\\ \frac{1}{\bar{R}}\left(A+\frac{B}{\bar{R}}\right)\frac{\mathrm{d}R_i^p(\tau_k)}{\mathrm{d}s}-\left(B+\frac{D}{\bar{R}}\right)\frac{\mathrm{d}^3R_i^p(\tau_k)}{\mathrm{d}s^3} & \frac{A}{\bar{R}^2}R_i^p(\tau_k)-\frac{2B}{\bar{R}}\frac{\mathrm{d}^2R_i^p(\tau_k)}{\mathrm{d}s^2}+D\frac{\mathrm{d}^4R_i^p(\tau_k)}{\mathrm{d}s^4}\end{bmatrix}\cdot\begin{pmatrix}\hat{u}_i\\ \hat{w}_i\end{pmatrix}=\begin{pmatrix}-p_u(\tau_j)\\ p_w(\tau_k)\end{pmatrix}, & \begin{matrix}j=3,4,\dots,n-2\\ k=2,4,\dots,n-1\end{matrix} \quad \text{(c)}\\
\displaystyle\sum_{i=1}^{m}\begin{bmatrix}\left(B+\frac{D}{\bar{R}}\right)\frac{\mathrm{d}^2R_i^p(\tau_n)}{\mathrm{d}s^2} & \frac{B}{\bar{R}}\frac{\mathrm{d}R_i^p(\tau_n)}{\mathrm{d}s}-D\frac{\mathrm{d}^3R_i^p(\tau_n)}{\mathrm{d}s^3}\end{bmatrix}\cdot\begin{pmatrix}\hat{u}_i\\ \hat{w}_i\end{pmatrix}=0, & \text{(d)}\\
\displaystyle\sum_{i=1}^{m}\begin{bmatrix}\left(A+\frac{B}{\bar{R}}\right)\frac{\mathrm{d}R_i^p(\tau_n)}{\mathrm{d}s} & \frac{A}{\bar{R}}R_i^p(\tau_n)-B\frac{\mathrm{d}^2R_i^p(\tau_n)}{\mathrm{d}s^2}\\ \left(B+\frac{D}{\bar{R}}\right)\frac{\mathrm{d}R_i^p(\tau_n)}{\mathrm{d}s} & \frac{B}{\bar{R}}R_i^p(\tau_n)-D\frac{\mathrm{d}^2R_i^p(\tau_n)}{\mathrm{d}s^2}\end{bmatrix}\cdot\begin{pmatrix}\hat{u}_i\\ \hat{w}_i\end{pmatrix}=\begin{pmatrix}0\\0\end{pmatrix}, & \text{(e)}
\end{cases}
\tag{32}
$$

Box I.

thickness h as

$$
\sigma_{sz}(z)=\frac{1}{\left(z+\bar{R}\right)^2}\left(\int_{\underline{z}}^{z}-\left(\left(z+\bar{R}\right)\bar{R}\,\sigma_{ss,s}(\zeta)+b_s(\zeta)\right)\mathrm{d}\zeta+\sigma_{sz}\left(\underline{z}\right)\right),
\tag{35}
$$

where $\underline{z}$ is chosen as the value of z at the bottom of the beam. It should be noted that integral (35) is computed numerically using a composite trapezoidal quadrature rule once the derivatives necessary for the recovery are evaluated as

$$
\begin{aligned}
\sigma_{ss,s}&=\frac{\mathrm{d}\mathbb{Q}_{11}}{\mathrm{d}s}\left(\varepsilon^0-zk^0\right)+\mathbb{Q}_{11}\left(\frac{\mathrm{d}\varepsilon^0}{\mathrm{d}s}-z\frac{\mathrm{d}k^0}{\mathrm{d}s}\right)\\
&=\mathbb{Q}_{11}\left(\left(\frac{\mathrm{d}^2u}{\mathrm{d}s^2}+\frac{1}{\bar{R}}\frac{\mathrm{d}w}{\mathrm{d}s}\right)-z\left(-\frac{1}{\bar{R}}\frac{\mathrm{d}^2u}{\mathrm{d}s^2}+\frac{\mathrm{d}^3w}{\mathrm{d}s^3}\right)\right),
\end{aligned}
\tag{36}
$$

having assumed, without loss of generality, that $\mathbb{Q}_{11}$ is constant for each layer along s, as it is in the case of homogeneous anisotropic materials (including orthotropic ones) in which the fibers have a constant orientation α with respect to the beam axis, and, consequently, the term $\frac{\mathrm{d}\mathbb{Q}_{11}}{\mathrm{d}s}$ vanishes.

With reference to Eqs. (35) and (36), it is clear that to apply the proposed post-processing technique, a highly regular displacement solution is needed. More specifically, the required derivatives need to be computed from a C^2-continuous displacement solution, which can be achieved using, e.g., isogeometric analysis.

5. Numerical tests

We now consider a quarter of curved cantilever beam that is clamped at one end ($s = 0$) and loaded with a tip force $F = 1$ in negative X_1-direction at $s = \bar{R}\pi/2$, being $\bar{R}$ the mean radius (see Fig. 2). The thickness of every single layer is set to 1 mm, and the mean radius $\bar{R}$ is S times larger than the total thickness of the laminate t, $S = \bar{R}/t$, while the base $b = t$. Thus, S represents the inverse of the slenderness parameter or mean radius-to-thickness ratio. Layer material parameters taken into account for all the proposed numerical tests are summarized for 0°-oriented plies in Table 1, whereas all stress profiles in the local reference system are then normalized as

$$
\overline{\sigma}_{ss}=\frac{\sigma_{ss}}{S^2},
\tag{37}
$$

$$
\overline{\sigma}_{sz}=\frac{\sigma_{sz}}{S}.
\tag{38}
$$

For this benchmark, we present and comment several numerical results investigating different types of cross-ply laminates featuring a 0°/90° stacking sequence starting from the bottom to the top of the composite. We model beams with $S = \{20, 50\}$ featuring both odd and even number of layers (i.e., # layers $= \{3, 4, 11, 14\}$) and, in Figs. 3 and 4, we show the good approximation of the normal stress profiles computed with $p = 6$, which fulfills the continuity requirements described in Section 4, and 16 knot spans for two distinct sampling points: $P_1 = 0.1\bar{R}\pi/2$, close to the clamped boundary, and $P_2 = 0.9\bar{R}\pi/2$, in the proximity of the Neumann's boundary. To study this beam problem, we consider both an IGA collocation method, whose strategy has been depicted in Section 3.3, as well as an IGA Galerkin approach, such that, to clamp the beam following [34], we impose that the displacement field of the first control point and the transverse displacement of the second control point are zero (i.e., $\hat{u}_1 = \hat{w}_1 = \hat{w}_2 = 0$). Following [78], the obtained transverse shear stresses are validated against an overkill 3D solid Finite Element Abaqus solution (version Abaqus/CAE 2023) comprising C3D20R elements (i.e., 20-node quadratic brick elements with reduced integration) as detailed for the considered varying number of layers and mean radius-to-thickness ratios in Table 2.

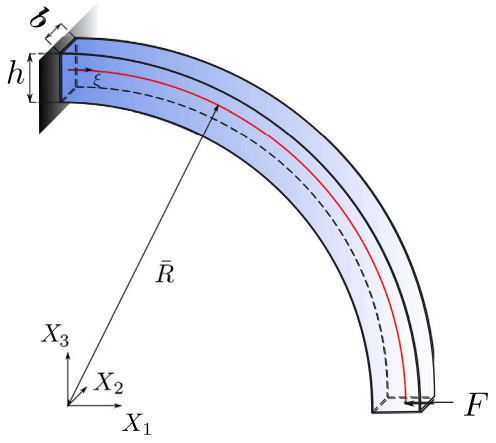

Fig. 2. Curved cantilever beam: geometry and boundary conditions.

Table 1
Material properties for 0°-oriented layers.

E_1 [GPa]	E_2 [GPa]	E_3 [GPa]	G_{23} [GPa]	G_{13} [GPa]	G_{12} [GPa]	ν_{23} [–]	ν_{13} [–]	ν_{12} [–]
25 000	1000	1000	0.2	0.5	0.5	0.25	0.25	0.25

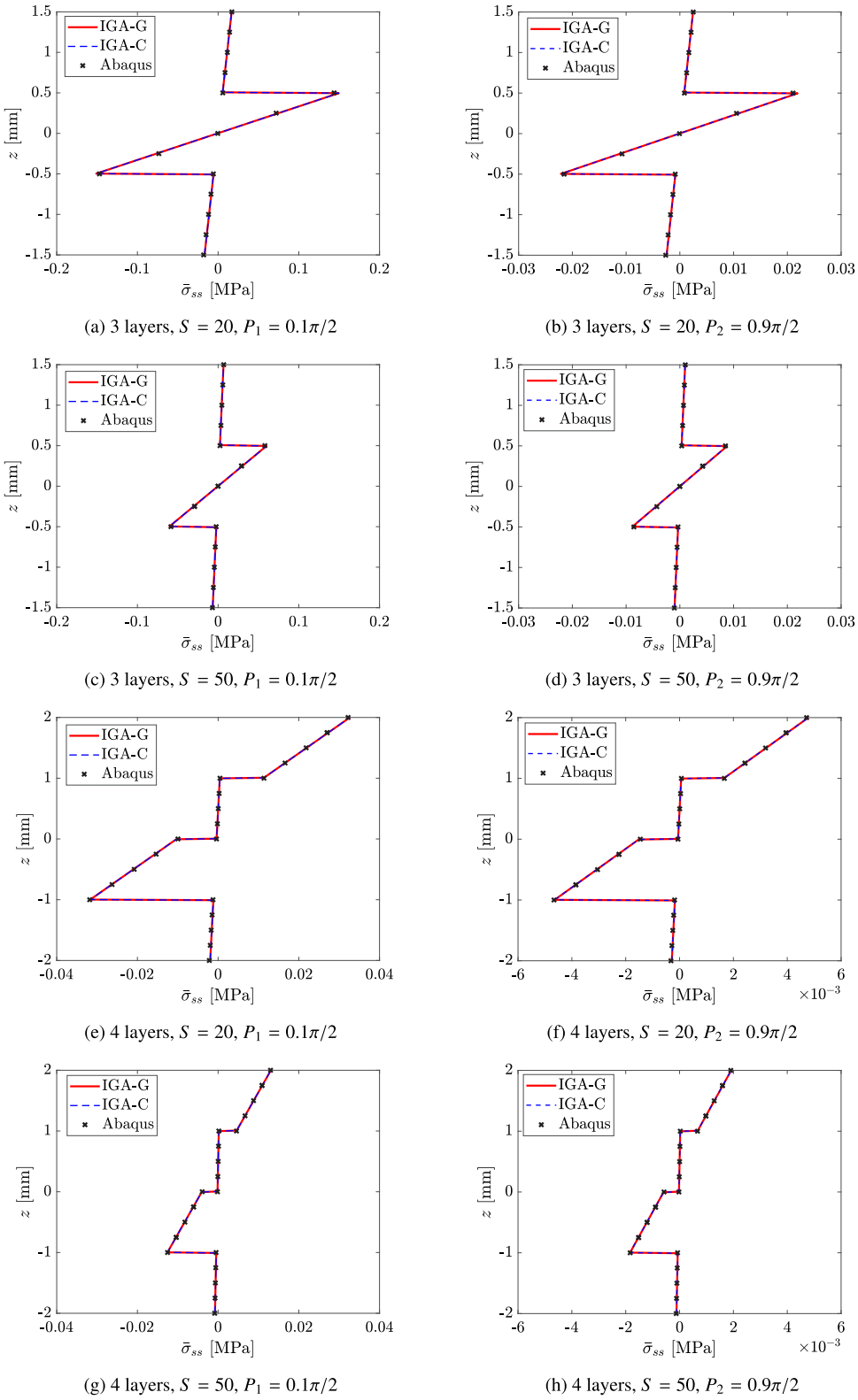

(a) 3 layers, $S = 20$, $P_1 = 0.1\pi/2$

(b) 3 layers, $S = 20$, $P_2 = 0.9\pi/2$

(c) 3 layers, $S = 50$, $P_1 = 0.1\pi/2$

(d) 3 layers, $S = 50$, $P_2 = 0.9\pi/2$

(e) 4 layers, $S = 20$, $P_1 = 0.1\pi/2$

(f) 4 layers, $S = 20$, $P_2 = 0.9\pi/2$

(g) 4 layers, $S = 50$, $P_1 = 0.1\pi/2$

(h) 4 layers, $S = 50$, $P_2 = 0.9\pi/2$

Fig. 3. Profiles of the normal stress through the beam thickness at different sampling locations considering structures with # layers = $\{3, 4\}$ and $S = \{20, 50\}$. Results obtained taking into account 16 knot spans and $p = 6$.

The normalized stresses obtained with either an IGA Galerkin or IGA collocation approach prove in all cases to accurately capture the behavior of both symmetric and antisymmetric cross-ply structures, as well as reproducing the ply-wise jumps happening at the interface level even for a rather small slenderness beam ratio (i.e., $S = 20$). Further tests have been carried out for the minimum degree requirement of the displacement field approximation (i.e., $p = 4$), leading to a less accurate solution for collocation. We acknowledge that the considered beam tests would, in principle, suffer from locking due to the curvature of the structure. However, in the isogeometric analysis framework, in

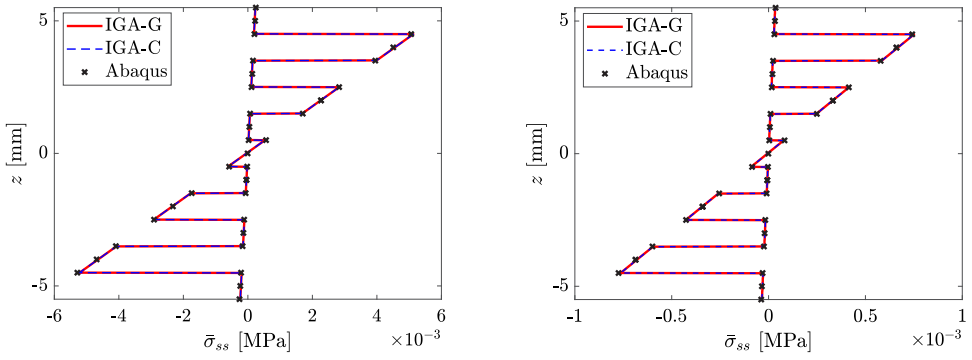

(a) 11 layers, $S = 20$, $P_1 = 0.1\pi/2$ (b) 11 layers, $S = 20$, $P_2 = 0.9\pi/2$

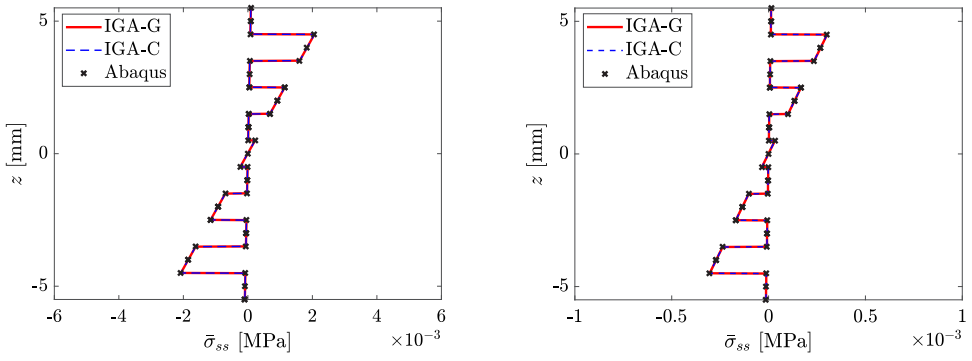

(c) 11 layers, $S = 50$, $P_1 = 0.1\pi/2$ (d) 11 layers, $S = 50$, $P_2 = 0.9\pi/2$

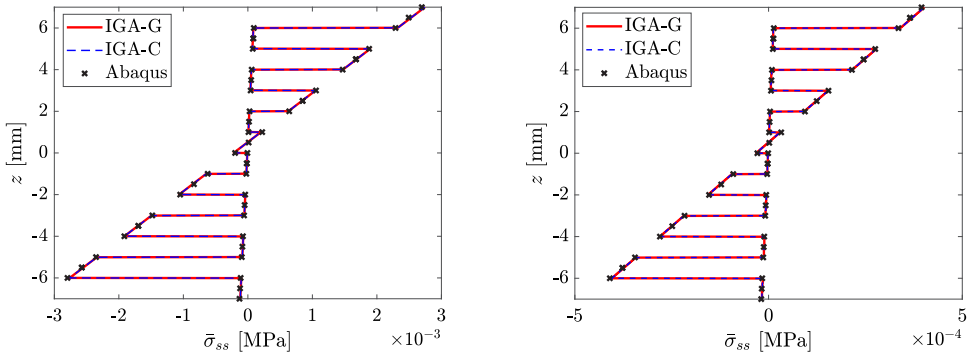

(e) 14 layers, $S = 20$, $P_1 = 0.1\pi/2$ (f) 14 layers, $S = 20$, $P_2 = 0.9\pi/2$

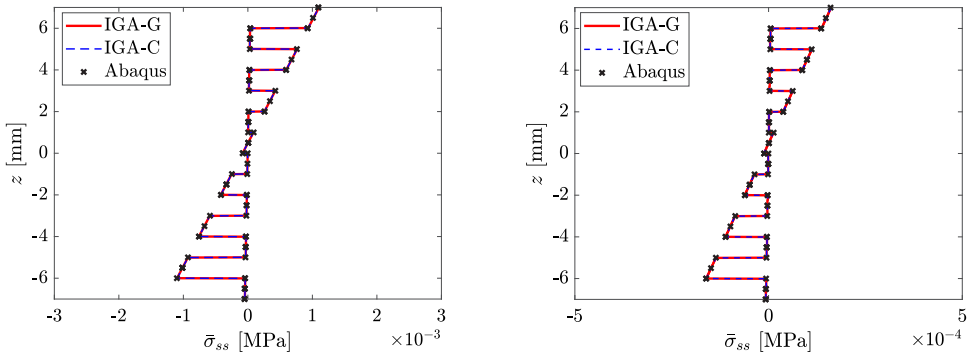

(g) 14 layers, $S = 50$, $P_1 = 0.1\pi/2$ (h) 14 layers, $S = 50$, $P_2 = 0.9\pi/2$

Fig. 4. Profiles of the normal stress through the beam thickness at different sampling locations considering structures with # layers = $\{11, 14\}$ and $S = \{20, 50\}$. Results obtained taking into account 16 knot spans and $p = 6$.

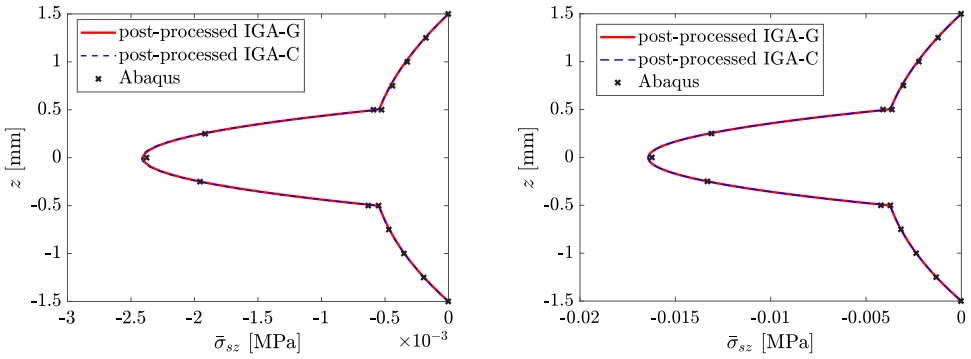

(a) 3 layers, $S = 20$, $P_1 = 0.1\pi/2$

(b) 3 layers, $S = 20$, $P_2 = 0.9\pi/2$

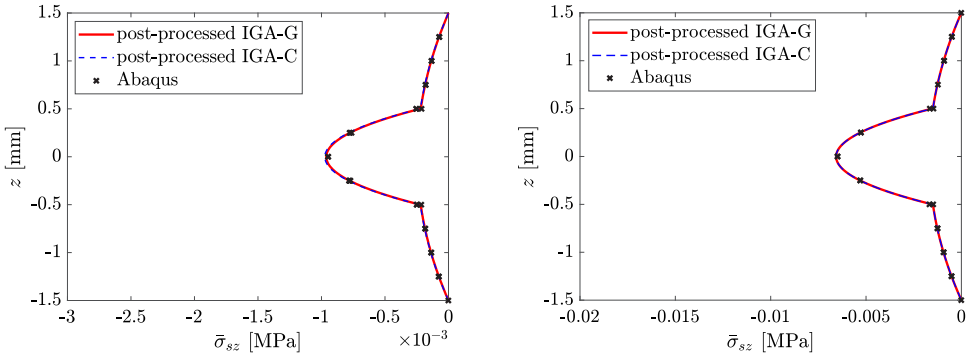

(c) 3 layers, $S = 50$, $P_1 = 0.1\pi/2$

(d) 3 layers, $S = 50$, $P_2 = 0.9\pi/2$

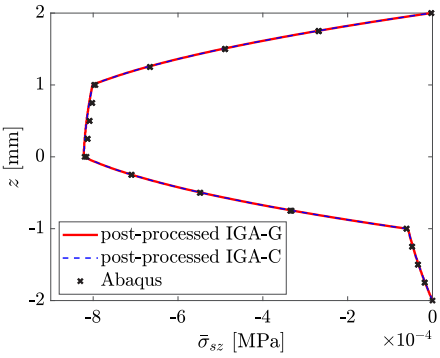

(e) 4 layers, $S = 20$, $P_1 = 0.1\pi/2$

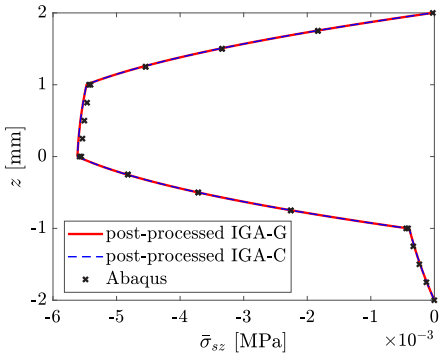

(f) 4 layers, $S = 20$, $P_2 = 0.9\pi/2$

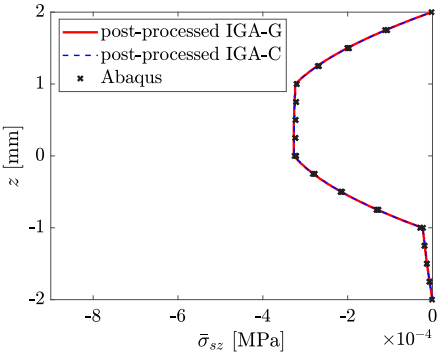

(g) 4 layers, $S = 50$, $P_1 = 0.1\pi/2$

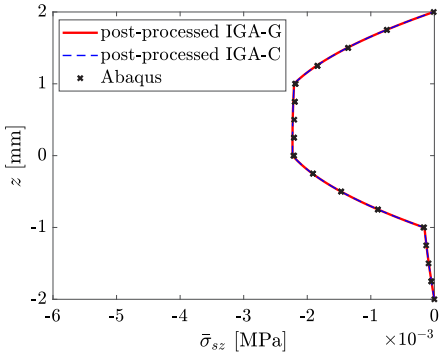

(h) 4 layers, $S = 50$, $P_2 = 0.9\pi/2$

Fig. 5. Profiles of the transverse shear stress through the beam thickness at different sampling locations considering structures with # layers = $\{3,4\}$ and $S = \{20,50\}$. Results obtained taking into account 16 knot spans and $p = 6$.

addition to the usual post-processing techniques to achieve smooth stress results, a simple way to alleviate locking is elevating the basis order (see, e.g., [79] and references therein). Specifically, in our work, we utilize approximation degree $p = 6$, which proved to be a reasonable

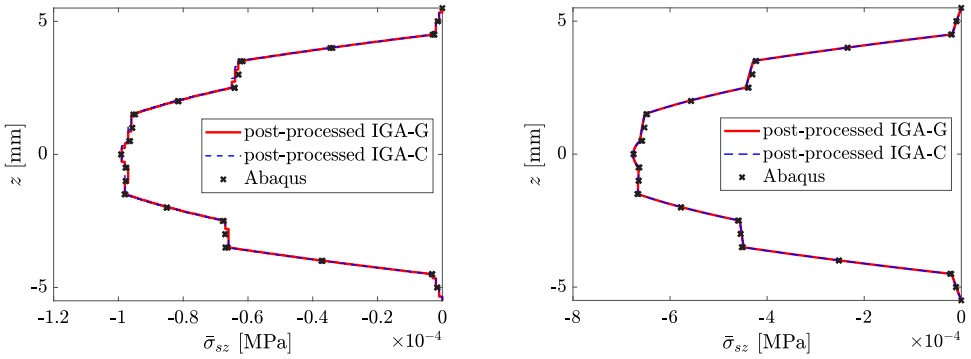

(a) 11 layers, $S = 20$, $P_1 = 0.1\pi/2$ (b) 11 layers, $S = 20$, $P_2 = 0.9\pi/2$

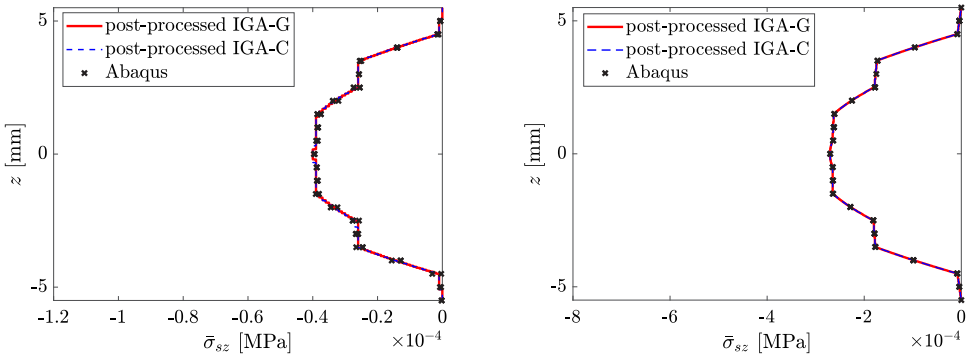

(c) 11 layers, $S = 50$, $P_1 = 0.1\pi/2$ (d) 11 layers, $S = 50$, $P_2 = 0.9\pi/2$

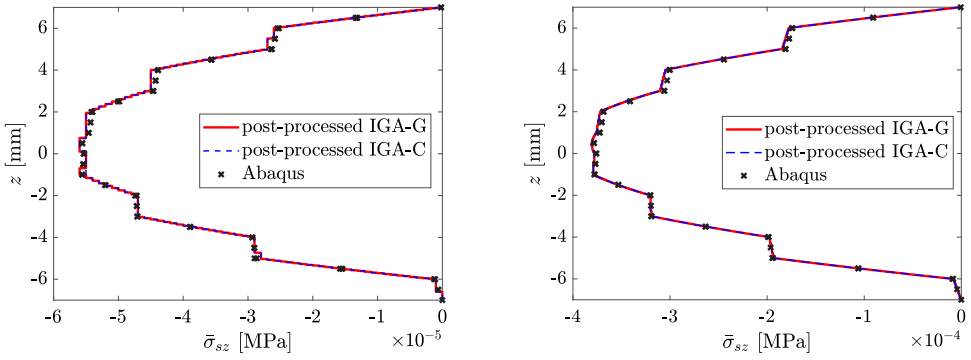

(e) 14 layers, $S = 20$, $P_1 = 0.1\pi/2$ (f) 14 layers, $S = 20$, $P_2 = 0.9\pi/2$

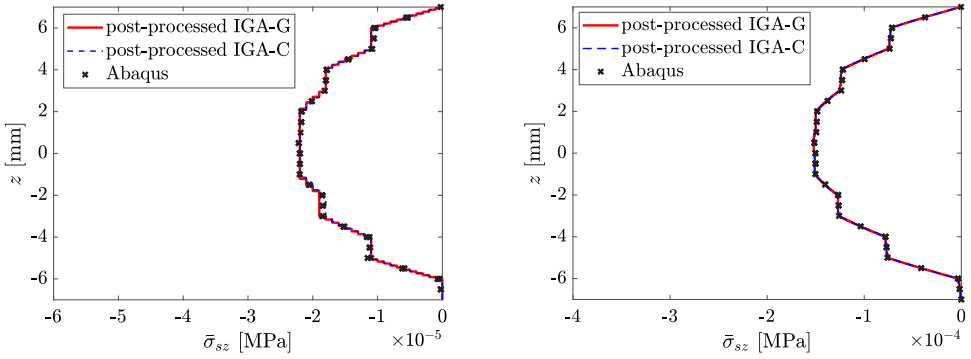

(g) 14 layers, $S = 50$, $P_1 = 0.1\pi/2$ (h) 14 layers, $S = 50$, $P_2 = 0.9\pi/2$

Fig. 6. Profiles of the transverse shear stress through the beam thickness at different sampling locations considering structures with # layers $= \{11, 14\}$ and $S = \{20, 50\}$. Results obtained taking into account 16 knot spans and $p = 6$.

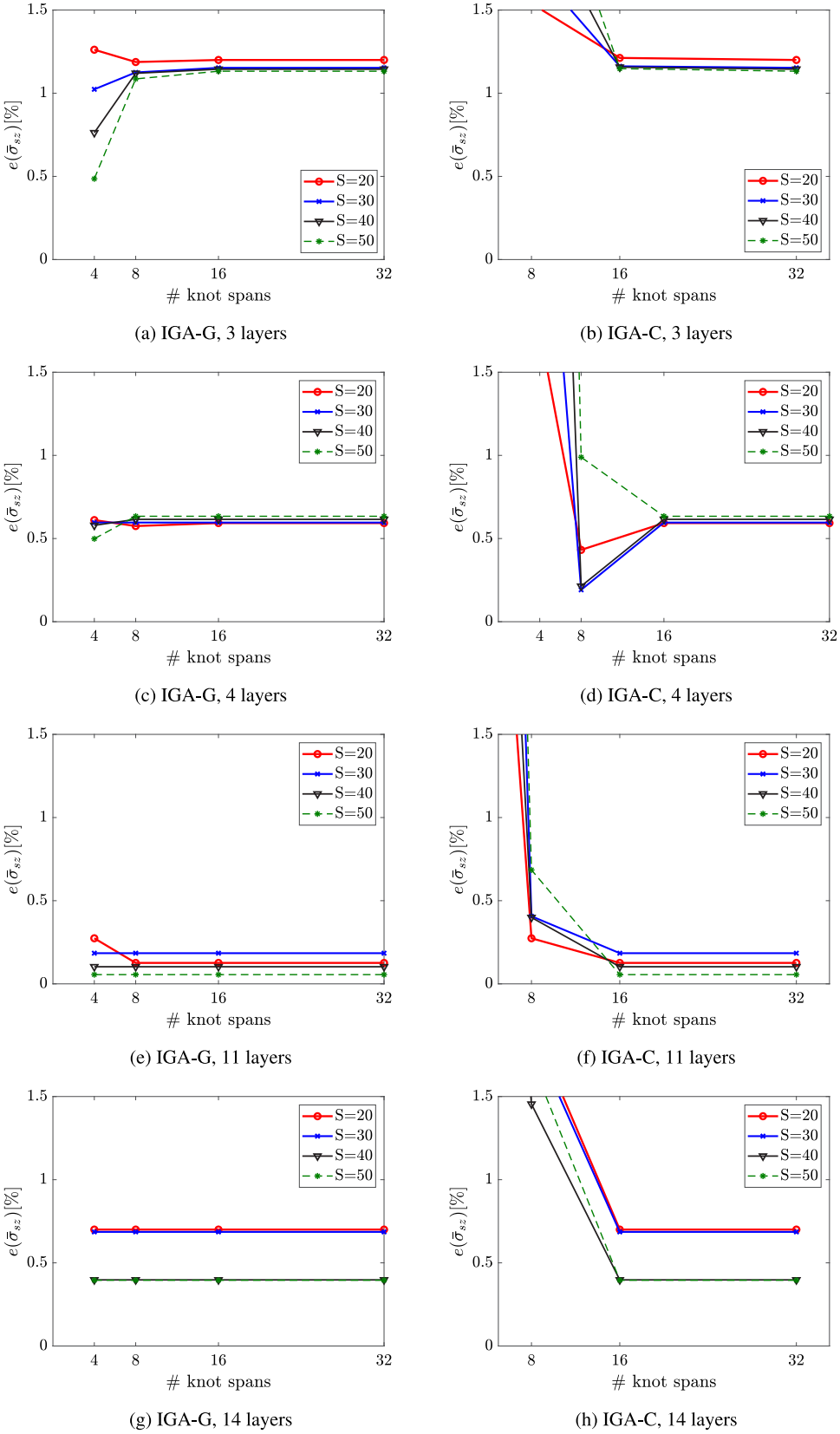

(a) IGA-G, 3 layers

(b) IGA-C, 3 layers

(c) IGA-G, 4 layers

(d) IGA-C, 4 layers

(e) IGA-G, 11 layers

(f) IGA-C, 11 layers

(g) IGA-G, 14 layers

(h) IGA-C, 14 layers

Fig. 7. Relative error of the maximum transverse shear stress value through the beam thickness for various slenderness parameters (i.e., $S = \{20, 30, 40, 50\}$) and different number of layers (namely # layers $= \{3, 4, 11, 14\}$) at $P_2 = 0.9\pi/2$ considering $p = 6$.

Table 2
Total number of C3D20R elements considered to build the overkill 3D solid Finite Element Abaqus solution for the examined number of layers and mean radius-to-thickness ratio.

	3 layers	4 layers	11 layers	33 layers
$S = 20$	55,584	81,216	108,432	135,504
$S = 30$	127,744	192,256	256,256	320,768
$S = 40$	330,572	497,552	665,016	831,996
$S = 50$	471,184	526,064	1,027,040	1,161,104

choice in line with [60,61] to obtain accurate results and correctly reproduce the beam interlaminar stress behavior for both considered discretization approaches.

5.1. The local stress recovery effect

For the same sampling points P_1 and P_2 and beam cases considered in Figs. 3 and 4, we now investigate the performance of the local stress recovery technique introduced in Section 4. Thus, starting from the obtained IGA-G and IGA-C displacement solutions, we are able to accurately reconstruct the transverse shear stress profiles in Figs. 5 and 6 by applying equilibrium equations directly at the locations of interest.

To further test the proposed approach, we investigate the convergence of several beam cases which consider a progressively larger slenderness ratio (i.e., $S = \{20, 30, 40, 50\}$) and 3, 4, 11, and 14 layers, examining an increasing number of degrees of freedom and an approximation degree $p = 6$. It is worth noticing that the process to build our overkill reference solution is rather expensive for laminates characterized by a high number of plies, as we utilize a layerwise approach (see, e.g., [80] and references therein) that necessarily needs 1 element to model each layer and namely 2 per ply to obtain accurate profile solutions in practice. Thus, in Fig. 7, we assess the convergence of both the IGA-G and the IGA-C approaches coupled with the presented post-processing technique at P_2, which corresponds to a point where the interlaminar transverse shear is more relevant for this benchmark and examine the relative error of the maximum value of this stress component along the beam thickness. In fact, after the post-processing step is applied, which is fundamental as we cannot directly assess interlaminar shear stresses using Euler–Bernoulli constitutive equations, we are able to obtain accurate results using both IGA-C and IGA-G even considering a relatively coarse mesh comprising 16 knot spans along the beam axis. Overall, the post-processing approach seems to be particularly suitable for tackling slender beams characterized by a significant number of layers. The error plots prove to be rather stable for the isogeometric Galerkin case starting from 8 knot spans, whereas for collocation, we need to consider 16 elements to encounter this type of behavior. In fact, after considering this level of refinement, we observe that the modeling error, given by the a posteriori step, dominates over the approximation one; thus, further refinement operations do not seem to provide a significant benefit in terms of accuracy for the considered tests, confirming what has been observed in [61,63]. More specifically, both IGA-G and IGA-C provide errors in the order of 0.7% or lower for # layers > 3, and even in the case of 3 layers, the error does not exceed 1.2%.

6. Conclusions

In this work, we extend the equilibrium-based stress recovery proposed in [60,63] to study the transverse shear behavior of laminated Euler–Bernoulli curved beams that do not provide a direct assessment of the interlaminar shear stress using constitutive relations. To this end, we first compute the displacement field solution in the curvilinear system convenient for the description of the beam, whose problem definition features high-order PDEs in primal form that can be easily approximated by leveraging IGA shape functions higher-continuity properties. In this work, we also consider the coupling between membrane and bending behavior, whereas in [60] we account for only bending behavior in the context of Kirchhoff's plates. A systematic reduction of the 3D composite constitutive relation is examined with exact integration through the laminate thickness to include the complete stacking sequence information in our formulation, which allows for an accurate solution utilizing both an isogeometric collocation and a Galerkin method. As the interlaminar shear stress is not directly available considering an Euler–Bernoulli formulation, we propose to perform a local stress recovery *via* simple numerical integration of curvilinear equilibrium equations. Given the chosen beam description, the high-order derivatives required for this *a posteriori* step are quantities already referred to the beam axis. As a result, the proposed approach avoids performing any change of coordinates, thereby providing an even more straightforward stress recovery for this simpler type of structure than in [63]. The accuracy of the proposed method is proven for both Galerkin and collocation approaches, considering either symmetric or non-symmetric ply distributions. Our numerical tests confirm the effectiveness of the proposed approach, particularly for slender laminated beams comprising a relevant number of layers.

Further research topics currently under investigation consider the extension of this approach to more complex variational formulations, such as Kirchhoff–Love shells, and the inclusion of material and geometrical nonlinearities. Moreover, among future study directions, we highlight that this formulation can be easily applied to investigate e.g., energy harvesting or mems devices from composite beams produced at different lamination.

CRediT authorship contribution statement

Alessia Patton: Writing – review & editing, Writing – original draft, Visualization, Validation, Software, Methodology, Investigation, Formal analysis, Conceptualization. **Shirko Faroughi:** Writing – review & editing, Writing – original draft, Visualization, Validation, Methodology, Formal analysis, Conceptualization. **Alessandro Reali:** Writing – review & editing, Visualization, Validation, Supervision, Methodology, Funding acquisition, Conceptualization.

Declaration of competing interest

The authors declare that they have no known competing financial interests or personal relationships that could have appeared to influence the work reported in this paper.

Data availability

The data that support the findings of this study are available from the authors upon reasonable request.

Acknowledgments

A. Reali is a member of the Gruppo Nazionale Calcolo Scientifico-Istituto Nazionale di Alta Matematica (GNCS-INDAM), and acknowledges the support of the Italian Ministry of University and Research (MUR) through the PRIN project COSMIC (No. 2022A79M75), funded by the European Union - Next Generation EU, as well as the contribution of the National Recovery and Resilience Plan, Mission 4 Component 2 - Investment 1.4 - NATIONAL CENTER FOR HPC, BIG DATA AND QUANTUM COMPUTING, spoke 6. Shirko Faroughi acknowledges the support of the Committee for international cooperation and development (CICOPS Scholarship) through the award of the Programme Grant with the University of the Pavia.

References

[1] Reddy JN. Mechanics of laminated composite plates and shells: theory and analysis. (2nd ed.). CRC Press; 2003.
[2] Gibson RF. Principles of composite material mechanics. (4th ed.). CRC Press; 2016.
[3] Yasin MY, Khalid HM, Beg MS. Exact solution considering layerwise mechanics for laminated composite and sandwich curved beams of deep curvatures. Compos Struct 2020;244:112258.
[4] Mittelstedt C, Becker W. Free-edge effects in composite laminates. Appl Mech Rev 2007;60:217–45.
[5] Sridharan S, Li Y, El-Sayed S. 21 - Delamination failure under compression of composite laminates and sandwich structures. In: Delamination behaviour of composites. Woodhead publishing series in composites science and engineering, Woodhead Publishing; 2008, p. 618–49.
[6] Uyar I, Arca MA, Gozluklu B, Coker D. Experimental observations of dynamic delamination in curved [0] and [0/90] composite laminates. Conf Proc Soc Exp Mech Ser 2015;66:189–96.
[7] Thurnherr C, Groh RMJ, Ermanni P, Weaver PM. Higher-order beam model for stress predictions in curved beams made from anisotropic materials. Int J Solids Struct 2016;97–98:16–28.
[8] Reddy JN. A simple higher-order theory for laminated composite plates. J Appl Mech 1984;51:745–52.
[9] Khdeir AA, Reddy JN. Free and forced vibration of cross-ply laminated composite shallow arches. Int J Solids Struct 1997;34:1217–34.
[10] Kim J-G. An effective composite laminated curved beam element. Commun Numer Methods Eng 2006;22:453–66.
[11] Ecsedi I, Dluhi K. A linear model for the static and dynamic analysis of non-homogeneous curved beams. Appl Math Model 2005;29:1211–31.
[12] Kant T, Pendhari SS, Desai YM. On accurate stress analysis of composite and sandwich narrow beams. Int J Comput Methods Eng Sci Mech 2007;8:165–77.
[13] Erkmen RE, Bradford MA. Nonlinear elastic analysis of composite beams curved in-plan. Eng Struct 2009;31:1613–24.
[14] Nguyen T-Q. Effects of curvature on the stresses of a curved laminated beams subjected to bending. 2010.
[15] Luu A-T, Kim N-I, Lee J. Bending and buckling of general laminated curved beams using NURBS-based isogeometric analysis. Eur J Mech A Solids 2015;54:218–31.
[16] Ye T, Jin G, Su Z. A spectral-sampling surface method for the vibration of 2-D laminated curved beams with variable curvatures and general restraints. Int J Mech Sci 2016;110:170–89.
[17] Mohamed N, Eltaher MA, Mohamed SA, Seddek LF. Numerical analysis of nonlinear free and forced vibrations of buckled curved beams resting on nonlinear elastic foundations. Int J Non-Linear Mech 2018;101:157–73.
[18] Guo J, Shi D, Wang Q, Pang F, Liang Q. A domain decomposition approach for static and dynamic analysis of composite laminated curved beam with general elastic restrains. Mech Adv Mater Struct 2019;26:1390–402.
[19] Hajianmaleki M, Qatu MS. Static and vibration analyses of thick, generally laminated deep curved beams with different boundary conditions. Composites B 2012;43:1767–75.
[20] Yasin MY, Khalid HM, Beg MS. Exact solution considering layerwise mechanics for laminated composite and sandwich curved beams of deep curvatures. Compos Struct 2020;244:112258.
[21] Avhad PV, Sayyad AS. On the deformation of laminated composite and sandwich curved beams. Curved Layer Struct 2022;9:1–12.
[22] Carrera E. Theories and finite elements for multilayered plates and shells: A unified compact formulation with numerical assessment and benchmarking. Arch Comput Methods Eng 2003;10:215–96.
[23] Carrera E, Pagani A, Petrolo M, Zappino E. Recent developments on refined theories for beams with applications. Mech Eng Rev 2015;2.
[24] Filippi M, Carrera E, Zenkour AM. Static analyses of FGM beams by various theories and finite elements. Composites B 2015;72:1–9.
[25] Kress G, Roos R, Barbezat M, Dransfeld C, Ermanni P. Model for interlaminar normal stress in singly curved laminates. Compos Struct 2005;69:458–69.
[26] Roos R, Kress G, Barbezat M, Ermanni P. Enhanced model for interlaminar normal stress in singly curved laminates. Compos Struct 2007;80:327–33.
[27] Cantero JM González, Díaz E Graciani, Carballo F París, Romano B López, Latova D. Semi-analytic solution on non-regularized unfolding stress in composite beams employing a series approximation based on Legendre polynomials. 2015.
[28] Kant T, Swaminathan K. Estimation of transverse/interlaminar stresses in laminated composites – a selective review and survey of current developments. Compos Struct 2000;49:65–75.
[29] Hughes TJR, Cottrell JA, Bazilevs Y. Isogeometric analysis: CAD, finite elements, NURBS, exact geometry and mesh refinement. Comput Methods Appl Mech Engrg 2005;194:4135–95.
[30] Dvořáková E, Patzák B. Isogeometric Bernoulli beam element with an exact representation of concentrated loadings. Comput Methods Appl Mech Engrg 2020;361:112745.
[31] Luu AT, Kim NI, Lee J. NURBS-based isogeometric vibration analysis of generally laminated deep curved beams with variable curvature. Compos Struct 2015;119:150–65.
[32] Faroughi S, Shafei E, Eriksson A. NURBS-based modeling of laminated composite beams with isogeometric displacement-only theory. Composites B 2019;162:89–102.
[33] Shafei E, Faroughi S, Reali A. Geometrically nonlinear vibration of anisotropic composite beams using isogeometric third-order shear deformation theory. Compos Struct 2020;252:112627.
[34] Marchiori G, Neto A. Isogeometric analysis applied to 2D Bernoulli–Euler beam model: imposition of constraints by Lagrange and penalty methods. Lat Am J Solids Struct 2020;17.
[35] Oesterle B, Bieber S, Sachse R, Ramm E, Bischoff M. Intrinsically locking-free formulations for isogeometric beam, plate and shell analysis. PAMM 2018;18:e201800399.
[36] Borković A, Marussig B, Radenković G. Geometrically exact static isogeometric analysis of arbitrarily curved plane Bernoulli–Euler beam. Thin-Walled Struct 2022;170:108539.
[37] Auricchio F, Calabrò F, Hughes TJR, Reali A, Sangalli G. A simple algorithm for obtaining nearly optimal quadrature rules for NURBS-based isogeometric analysis. Comput Methods Appl Mech Engrg 2012;249–252:15–27.
[38] Fahrendorf F, De Lorenzis L, Gomez H. Reduced integration at superconvergent points in isogeometric analysis. Comput Methods Appl Mech Engrg 2018;328:390–410.
[39] Sangalli G, Tani M. Matrix-free weighted quadrature for a computationally efficient isogeometric k-method. Comput Methods Appl Mech Engrg 2018;338:117–33.
[40] Schillinger D, Evans JA, Reali A, Scott MA, Hughes TJR. Isogeometric collocation: Cost comparison with Galerkin methods and extension to adaptive hierarchical NURBS discretizations. Comput Methods Appl Mech Engrg 2013;267:170–232.
[41] Reali A, Gomez H. An isogeometric collocation approach for Bernoulli–Euler beams and Kirchhoff plates. Comput Methods Appl Mech Engrg 2015;284:623–36.
[42] Kiendl J, Auricchio F, Reali A. A displacement-free formulation for the Timoshenko beam problem and a corresponding isogeometric collocation approach. Meccanica 2018;53:1403–13.
[43] Beirão da Veiga L, Lovadina C, Reali A. Avoiding shear locking for the Timoshenko beam problem via isogeometric collocation methods. Comput Methods Appl Mech Engrg 2012;241–244:38–51.
[44] Balduzzi G, Morganti S, Auricchio F, Reali A. Non-prismatic Timoshenko-like beam model: Numerical solution via isogeometric collocation. Comput Math Appl 2017;74:1531–41.
[45] Auricchio F, Beirão da Veiga L, Kiendl J, Lovadina C, Reali A. Locking-free isogeometric collocation methods for spatial Timoshenko rods. Comput Methods Appl Mech Engrg 2013;263:113–26.
[46] Kiendl J, Auricchio F, Hughes TJR, Reali A. Single-variable formulations and isogeometric discretizations for shear deformable beams. Comput Methods Appl Mech Engrg 2015;284:988–1004.
[47] Marino E. Locking-free isogeometric collocation formulation for three-dimensional geometrically exact shear-deformable beams with arbitrary initial curvature. Comput Methods Appl Mech Engrg 2017;324:546–72.
[48] Marino E, Kiendl J, De Lorenzis L. Explicit isogeometric collocation for the dynamics of three-dimensional beams undergoing finite motions. Comput Methods Appl Mech Engrg 2019;343:530–49.
[49] Marino E, Kiendl J, De Lorenzis L. Isogeometric collocation for implicit dynamics of three-dimensional beams undergoing finite motions. Comput Methods Appl Mech Engrg 2019;356:548–70.
[50] Weeger O, Yeung S-K, Dunn ML. Isogeometric collocation methods for Cosserat rods and rod structures. Comput Methods Appl Mech Engrg 2017;316:100–22.
[51] Weeger O, Yeung S-K, Dunn ML. Fully isogeometric modeling and analysis of nonlinear 3D beams with spatially varying geometric and material parameters. Comput Methods Appl Mech Engrg 2018;342:95–115.
[52] Marino E, Hosseini SF, Hashemian A, Reali A. Effects of parameterization and knot placement techniques on primal and mixed isogeometric collocation formulations of spatial shear-deformable beams with varying curvature and torsion. Comput Math Appl 2020;80:2563–85.
[53] Ignesti D, Ferri G, Auricchio F, Reali A, Marino E. An improved isogeometric collocation formulation for spatial multi-patch shear-deformable beams with arbitrary initial curvature. Comput Methods Appl Mech Engrg 2023;403:115722.
[54] Ferri G, Ignesti D, Marino E. An efficient displacement-based isogeometric formulation for geometrically exact viscoelastic beams. Comput Methods Appl Mech Engrg 2023;417:116413.
[55] Weeger O, Schillinger D, Müller R. Mixed isogeometric collocation for geometrically exact 3D beams with elasto-visco-plastic material behavior and softening effects. Comput Methods Appl Mech Engrg 2022;399:115456.
[56] Dufour J-E, Antolín P, Sangalli G, Auricchio F, Reali A. A cost-effective isogeometric approach for composite plates based on a stress recovery procedure. Composites B 2018;138:12–8.
[57] Engblom JJ, Ochoa OO. Through-the-thickness stress predictions for laminated plates of advanced composite materials. Internat J Numer Methods Engrg 1985;21:1759–76.
[58] Ubertini F. Patch recovery based on complementary energy. Internat J Numer Methods Engrg 2004;59:1501–38.

[59] Daghia F, de Miranda S, Ubertini F, Viola E. A hybrid stress approach for laminated composite plates within the first-order shear deformation theory. Int J Solids Struct 2008;45:1766–87.
[60] Patton A, Antolín P, Dufour J-E, Kiendl J, Reali A. Accurate equilibrium-based interlaminar stress recovery for isogeometric laminated composite Kirchhoff plates. Compos Struct 2021;256:112976.
[61] Patton A, Carraturo M, Auricchio F, Reali A. Cost-effective and accurate interlaminar stress modeling of composite Kirchhoff plates via immersed isogeometric analysis and equilibrium. J. Mech. 2022;38:32–43.
[62] Patton A, Dufour J-E, Antolín P, Reali A. Fast and accurate elastic analysis of laminated composite plates via isogeometric collocation and an equilibrium-based stress recovery approach. Compos Struct 2019;225:111026.
[63] Patton A, Antolín P, Kiendl J, Reali A. Efficient equilibrium-based stress recovery for isogeometric laminated curved structures. Compos Struct 2021;272:113975.
[64] Chiappa A, Groth C, Reali A, Biancolini ME. A stress recovery procedure for laminated composite plates based on strong-form equilibrium enforced via the RBF Kansa method. Compos Struct 2020;244:112292.
[65] Vo D, Li X, Nanakorn P, Bui TQ. An efficient isogeometric beam formulation for analysis of 2D non-prismatic beams. Eur J Mech A Solids 2021;89:104280.
[66] Balduzzi G, Morganti S, Füssl J, Aminbaghai M, Reali A, Auricchio F. Modeling the non-trivial behavior of anisotropic beams: A simple Timoshenko beam with enhanced stress recovery and constitutive relations. Compos Struct 2019;229:111265.
[67] Mercuri V, Balduzzi G, Asprone D, Auricchio F. Structural analysis of non-prismatic beams: Critical issues, accurate stress recovery, and analytical definition of the finite element (FE) stiffness matrix. Eng Struct 2020;213:110252.
[68] Bardella L. Explicit analytical solutions for the full plane-stress field in sandwich beams under flexure governed by zigzag warping. Compos Struct 2024;329:117754.
[69] Bhimaraddi A, Chandrashekhara K. Some observations on the modeling of laminated composite beams with general lay-ups. Compos Struct 1991;19:371–80.
[70] Oden JT. Mechanics of elastic structures. (1st ed.). McGraw-Hill; 1967.
[71] Bucalem ML, Bathe K-J. Mathematical models and the finite element solution. Hierarchical modeling. In: The mechanics of solids and structures - hierarchical modeling and the finite element solution. Berlin, Heidelberg: Springer Berlin Heidelberg; 2011, p. 1–17.
[72] Cottrell JA, Hughes TJR, Reali A. Studies of refinement and continuity in isogeometric structural analysis. Comput Methods Appl Mech Engrg 2007;196:4160–83.
[73] Boor C De. On calculation with B-splines. J Approx Theory 1972;6:50–62.
[74] Auricchio F, da Veiga L Beirão, Hughes TJR, Reali A, Sangalli G. Isogeometric collocation for elastostatics and explicit dynamics. Comput Methods Appl Mech Engrg 2012;249–252:2–14.
[75] De Lorenzis L, Evans JA, Hughes TJR, Reali A. Isogeometric collocation: Neumann boundary conditions and contact. Comput Methods Appl Mech Engrg 2015;284:21–54.
[76] Johnson RW. A B-spline collocation method for solving the incompressible Navier–Stokes equations using an ad hoc method: The boundary residual method. Comput & Fluids 2005;34:121–49.
[77] Demko S. On the existence of interpolating projections onto spline spaces. J Approx Theory 1985;43:151–6.
[78] Fagiano C, Abdalla MM, Kassapoglou C, Gürdal Z. Interlaminar stress recovery for three-dimensional finite elements. Compos Sci Technol 2010;70:530–8.
[79] Zou Z, Hughes TJR, Scott MA, Sauer RA, Savitha EJ. Galerkin formulations of isogeometric shell analysis: Alleviating locking with Greville quadratures and higher-order elements. Comput Methods Appl Mech Engrg 2021;380:113757.
[80] Li D. Layerwise theories of laminated composite structures and their applications: A review. Arch Comput Methods Eng 2021;28:577–600.